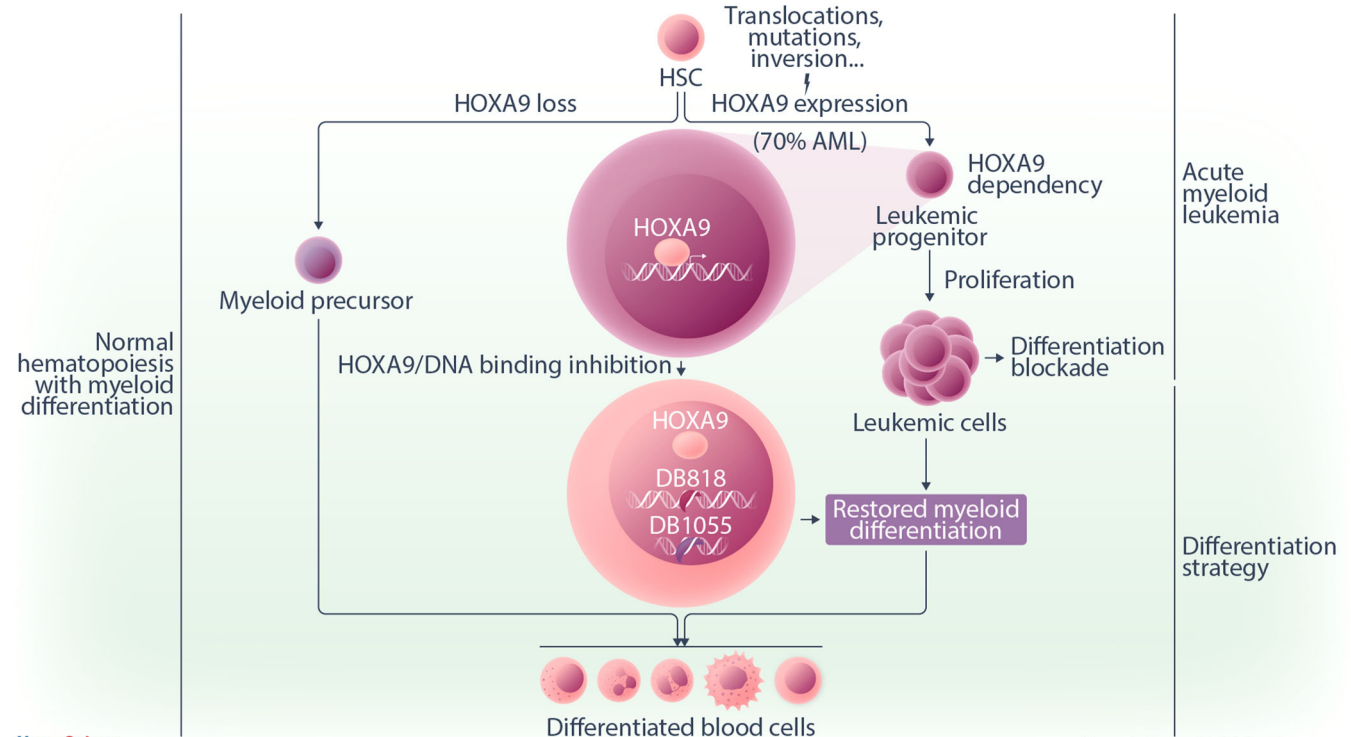




# Induction of AML cell differentiation using HOXA9/DNA binding inhibitors as a potential therapeutic option for HOXA9-dependent AML

Mélanie Lambert<sup>1,2</sup> | Samy Jambon<sup>1</sup> | Mohamed A. Bouhlel<sup>1</sup> | Sabine Depauw<sup>1</sup> | Julie Vrevin<sup>1</sup> | Samuel Blanck<sup>3,4</sup>  | Guillemette Marot<sup>3,4,5</sup> | Martin Figeac<sup>6</sup> | Claude Preudhomme<sup>1</sup> | Bruno Quesnel<sup>1</sup> | David W. Boykin<sup>7</sup> | Marie-Hélène David-Cordonnier<sup>1</sup> 

## Graphical Abstract



# Induction of AML cell differentiation using HOXA9/DNA binding inhibitors as a potential therapeutic option for HOXA9-dependent AML

Mélanie Lambert<sup>1,2</sup> | Samy Jambon<sup>1</sup> | Mohamed A. Bouhlel<sup>1</sup> | Sabine Depauw<sup>1</sup> | Julie Vrevin<sup>1</sup> | Samuel Blanck<sup>3,4</sup>  | Guillemette Marot<sup>3,4,5</sup> | Martin Figeac<sup>6</sup> | Claude Preudhomme<sup>1</sup> | Bruno Quesnel<sup>1</sup> | David W. Boykin<sup>7</sup> | Marie-Hélène David-Cordonnier<sup>1</sup> 

Correspondence: Marie-Hélène David-Cordonnier ([marie-helene.david@inserm.fr](mailto:marie-helene.david@inserm.fr))

## Abstract

The mainstay of acute myeloid leukemia (AML) treatment still relies on traditional chemotherapy, with a survival rate of approximately 30% for patients under 65 years of age and as low as 5% for those beyond. This unfavorable prognosis primarily stems from frequent relapses, resistance to chemotherapy, and limited approved targeted therapies for specific AML subtypes. Around 70% of all AML cases show overexpression of the transcription factor HOXA9, which is associated with a poor prognosis, increased chemoresistance, and higher relapse rates. However, direct targeting of HOXA9 in a clinical setting has not been achieved yet. The dysregulation caused by the leukemic HOXA9 transcription factor primarily results from its binding activity to DNA, leading to differentiation blockade. Our previous investigations have identified two HOXA9/DNA binding competitors, namely DB1055 and DB818. We assessed their antileukemic effects in comparison to HOXA9 knockdown or cytarabine treatment. Using human AML cell models, DB1055 and DB818 induced in vitro cell growth reduction, death, differentiation, and common transcriptomic deregulation but did not impact human CD34+ bone marrow cells. Furthermore, DB1055 and DB818 exhibited potent antileukemic activities in a human THP-1 AML in vivo model, leading to the differentiation of monocytes into macrophages. In vitro assays also demonstrated the efficacy of DB1055 and DB818 against AML blasts from patients, with DB1055 successfully reducing leukemia burden in patient-derived xenografts in NSG immunodeficient mice. Our findings indicate that inhibiting HOXA9/DNA interaction using DNA ligands may offer a novel differentiation therapy for the future treatment of AML patients dependent on HOXA9.

## INTRODUCTION

Acute myeloid leukemia (AML), characterized by higher proliferative activity and differentiation blockage of immature myeloid cells, lacks effective treatments despite advancements in understanding its subtypes. Current therapies rely on aggressive chemotherapy combining cytarabine (Ara-C) with anthracyclines or resorting to hematopoietic stem cell transplantation. However, these approaches

show limited efficacy, especially in patients over 60 with success rates dropping to 5%–15%, and a substantial relapse rate.<sup>1,2</sup>

With still over 50% of AML patients succumbing to the disease, exploring alternative therapeutic options is imperative to improve prognosis. Among approved or clinically tested targeted therapies are FLT3-mutated, P53-mutated, IDH-mutated or BCL2 inhibitors, cereblon E3-ligase modulators, and monoclonal antibodies (anti-CD33, CD123 ± CD3, CD47, CTLA4, PD-1, or TIM3).<sup>3,4</sup> Additionally,

<sup>1</sup>Univ. Lille, CNRS, Inserm, CHU Lille, IRCL, UMR9020-U1277–Canther–Cancer Heterogeneity, Plasticity and Resistance to Therapies, Lille, France

<sup>2</sup>Université Sorbonne Paris Nord, Bobigny, France

<sup>3</sup>Univ. Lille, CHU Lille, ULR 2694–METRICS, Lille, France

<sup>4</sup>Univ. Lille, CNRS, Inserm, CHU Lille, Institut Pasteur de Lille, US 41–UAR 2014–PLBS, Billille, Lille, France

<sup>5</sup>Inria, MODAL: Models for Data Analysis and Learning, Lille, France

<sup>6</sup>Plateau de Génomique Fonctionnelle et Structurale, CHU Lille, Univ. Lille, France, Lille, France

<sup>7</sup>Department of Chemistry, Georgia State University, Atlanta, Georgia, USA

This is an open access article under the terms of the [Creative Commons Attribution-NonCommercial-NoDerivs](https://creativecommons.org/licenses/by-nc-nd/4.0/) License, which permits use and distribution in any medium, provided the original work is properly cited, the use is non-commercial and no modifications or adaptations are made.

© 2024 The Authors. *HemaSphere* published by John Wiley & Sons Ltd on behalf of European Hematology Association.

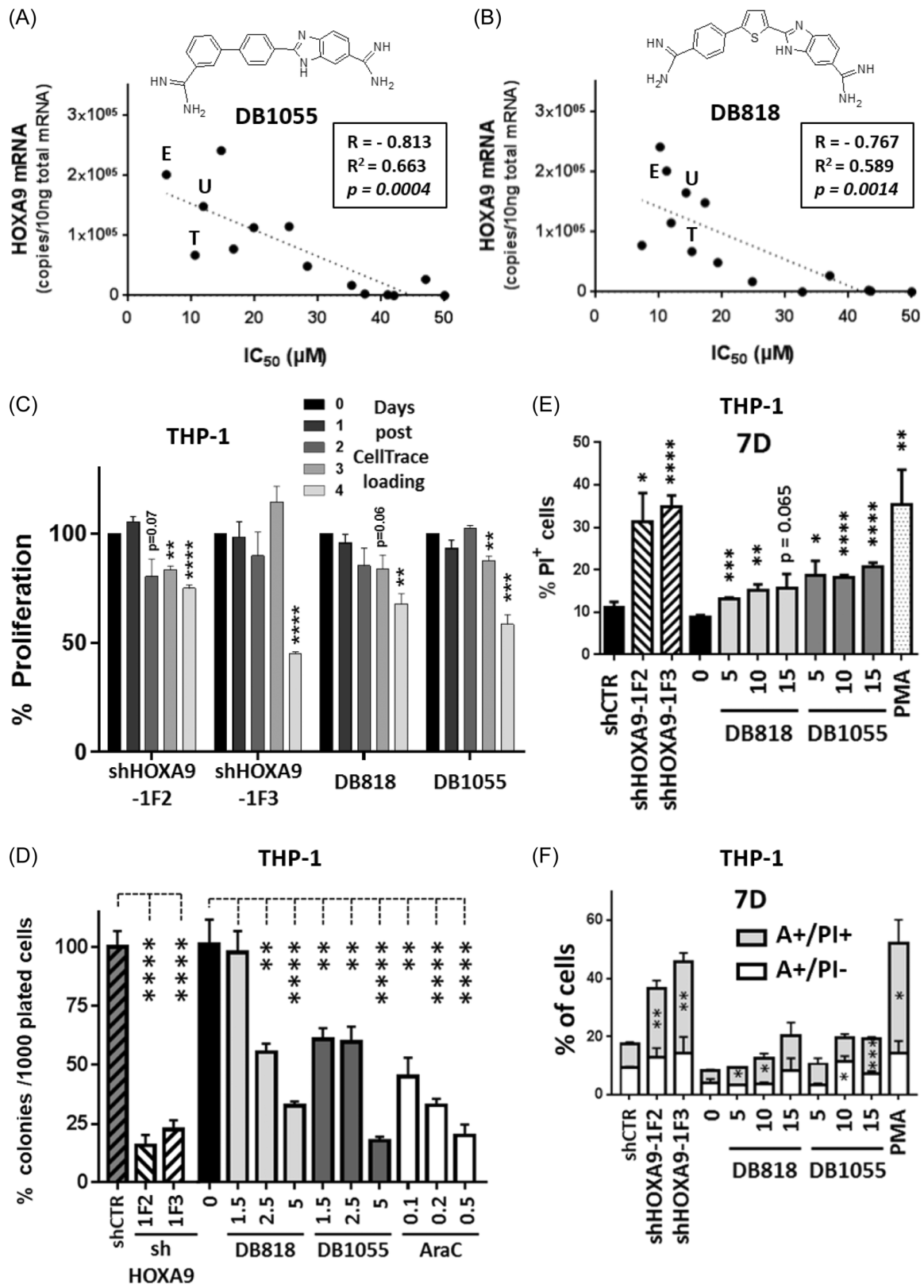


**FIGURE 1** (See caption on next page).

**FIGURE 1** DB1055 and DB818 affect cell survival in human HOXA9-positive acute myeloid leukemia (AML) cells and induce cell death. (A, B) Cell viability measurement upon treatment of DB818 or DB1055 on 14 human AML cell lines relative to their level of HOXA9 gene expression. Mean IC<sub>50</sub> values (CellTiter 96® AQueous One Solution Cell Proliferation Assay kit) are plotted over HOXA9 expression (absolute quantitative reverse-transcription polymerase chain reaction quantification relative to TBP, normalized to 10 ng of total purified messenger RNA). Linear regression curves are plotted. Corresponding R (coefficient of determination), R<sup>2</sup> (coefficient of correlation), and p-values are embedded. T, THP1; E, Eo1-1; U, U937 cell lines. (C) Quantification of relative cell proliferation using CellTrace™ loaded THP-1 cells. For HOXA9 invalidation, cells were transduced (~98% GFP-positive transduced cells) with lentivirus expressing shHOXA9-1F2, -1F3, or shCTR and washed prior to being loaded for 5 min with CellTrace™-Violet and washed prior to cell culture. For drug treatments, cells were loaded with CellTrace™-CFSE (compatible with drug intrinsic fluorescence) for 5 min and washed prior to the addition of 10 μM of DB1055 or DB818 or none. Each treatment was performed in triplicate. Cells were analyzed at the indicated days by flow cytometry. Graphs are expressed as the % of proliferation, normalized to the corresponding control (untreated or shCTR). (D) Effect of DB818 or DB1055 treatment or HOXA9 invalidation on colony-forming assays in THP-1 model. THP-1 cells were transduced with short hairpin RNA (shRNA) expressing lentivirus or treated with increasing concentrations of DB818, DB1055, or AraC treatment (μM) prior to being plated at a density of 1000 cells/well for 14 days (n = 6). Results are expressed as the percentage of colonies each well relative to the corresponding controls (shCTR or untreated "0." (E) Cell death induction analysis was evidenced using propidium iodide (PI) staining. THP-1 cells were transduced with shRNA expressing lentiviruses or treated with either DB818, DB1055 (μM), or PMA as a positive control (2.5 ng/mL) for 7 days prior to PI staining of dead cells and flow cytometry analysis (n = 6). (F) Apoptotic cell death induction was analyzed by Annexin V and PI double staining. Similarly treated cells were grown for 7 days prior to AnnexinV/PI labeling and flow cytometry analyses. Additive columns represent the percentage of annexinV-positive cells being also either PI-positive staining in gray or PI-negative in white (n = 6). Student t-test: \*\*\*\*p < 0.0001; \*\*\*p < 0.001; \*\*p < 0.01; \*p < 0.05; or as specified on graphs.

the development of small molecule inhibitors aiming to induce AML cell differentiation to mirror the success of *all-trans-retinoic-acid* (ATRA/Tretinoïne/Vesanoid®) and arsenic trioxide (ATO/Trisenox®) targeting the PML-RARα fusion transcription factor in acute promyelocytic leukemia (APL, AML-M3) is an attractive strategy leading to the development of IDH1 (Ivosidenib/AG-120/Tibsovo®) or IDH2 (Enasidenib/AG-221/Idhifa®) mutants inhibitors, or epigenetic modulators against the menin/MLL interaction like Revumenib/SNDX-5613, Ziftomenib/KO-539 or JNJ-6617, or targeting DOT1L histone methyltransferase (Pinometostat/EPZ-5676).<sup>5-7</sup>

While transcription factors play a key role in regulating the expression of oncogenic-associated genes, the direct targeting of these factors by antitumor molecules remains limited.<sup>8,9</sup> Notably, HOXA9 emerges as a crucial transcription factor in AML, exhibiting overexpression in ~70% of AML cases, including NPM1-mutated, MLL-rearranged, NUP98-NSD1, MYST3-CREBBP, RUNX1-EVI1, and EZH2-mutated AMLs. It is also directly involved in t(7;11)(p15;p15) translocation, leading to the NUP98-HOXA9 fusion protein observed in ~2% AML and ~5% of myelodysplastic syndromes.<sup>10-12</sup> HOXA9 is associated with poor/intermediate prognosis groups, treatment failure, and frequent relapse in patients.<sup>13,14</sup> Its overexpression correlates with the blockade of differentiation and apoptosis, and hematopoietic cell proliferation.<sup>15,16</sup> Presently, no specific small molecule inhibitor of HOXA9 is yet available. However indirect inhibitors primarily target its expression by focusing on proteins within the MLL complex, such as DOT1L, menin, WDR5, and other epigenetic regulators.<sup>10,17,18</sup> Additionally, there are attempts to directly target multiple HOX proteins, including HOXA9, along with their co-factors of the PBX family at the protein/protein interaction level (HXR9 peptidomimetic) developed against a variety of solid tumors and hematologic malignancies.<sup>19,20</sup>

Given the critical role of HOXA9 DNA binding in its leukemic impact, we previously screened numerous sequence-specific DNA ligands for similar recognition.<sup>21</sup> Heterocyclic diamidines initially designed for combating *Pneumocystis carinii*-associated pneumonia, leishmaniasis, malaria, or trypanosomiasis include DB289 (parafuramidine), a prodrug of DB75 (furamidine/Pentacarinat®). DB289, with an affinity for unspecific AT-rich sites, reached phase III clinical trials for human African trypanosomiasis and malaria.<sup>22</sup> Certain members of this heterocyclic diamidine family proved effective as sequence-selective transcription factor competitors targeting Pit-1/Brn-3,<sup>23</sup> Erg,<sup>24</sup> and PU.1.<sup>25</sup> Pretreating AML cells with PU.1 inhibitor, followed by engraftment in immunodeficient mice, resulted in reduced tumor burden and increased survival, suggesting the

potential of DNA-binding transcription factor inhibition as a therapeutic strategy.<sup>26</sup> Previously, we screened for their ability to compete with HOXA9 binding to DNA, focusing on their interaction with the HOXA9 cognate sequence 5'-ATTTA<sup>27</sup> DB1055 and DB818 were further studied *in vitro* in a murine *Hoxa9*-transformed cell line, evidencing cell death and differentiation and disruption of gene expression associated with leukemia such as *Akap13* associated with a decrease in HOXA9 binding to its gene regulatory sequence.<sup>21</sup> Furthermore, DB818 evidenced some antiproliferative effects on some AML cell lines, including apoptosis and slight, yet unquantified, differentiation in a THP-1 AML cell model.<sup>28</sup>

This study systematically contrasts the functional inhibition of HOXA9 achieved by DB1055 and DB818 with the effects of HOXA9 expression knockdown. Employing a comprehensive approach encompassing molecular, cellular, and *in vivo* experiments conducted on human AML cell models and primary patient samples, our findings unveil shared alterations in gene expression, consistent cellular outcomes in terms of death and differentiation, and robust antileukemic activities. Importantly, these effects are achieved with minimal impact on normal hematopoiesis. The outcomes from DB1055 and DB818 underscore their innovative potential as agents for AML differentiation therapy.

## MATERIALS AND METHODS

### Compounds, antibodies, DNA, and vectors

DB818 and DB1055 (Figure 1) were prepared at 10 mM and aliquoted at -20°C. For mice studies, DB818/1055 and AraC were dissolved in an isotonic saline solution. Antibodies and oligonucleotides (Eurogentec) are presented in Supporting Information Tables S1 and S2, respectively. The short hairpin RNA (shRNA) directed against HOXA9 shHOXA9-1F2 or -1F3<sup>26</sup> were subcloned in the shLuc-pRRL lentiviral vector used as control (Prof. Bob Weinberg, #19125; Addgene).<sup>29</sup>

### Cellular analyses

Cell lines and culture conditions are described in Supporting Information Methods. THP-1 cells were treated with DB818/1055, phorbol-12-myristate-13-acetate (PMA, 2.5 ng/mL) or AraC (10 μM), or transduced with lentiviruses expressing shHOXA9-1F2, shHOXA9-1F3, or a control sequence (shCTR). The lentiviral vector co-expressed the

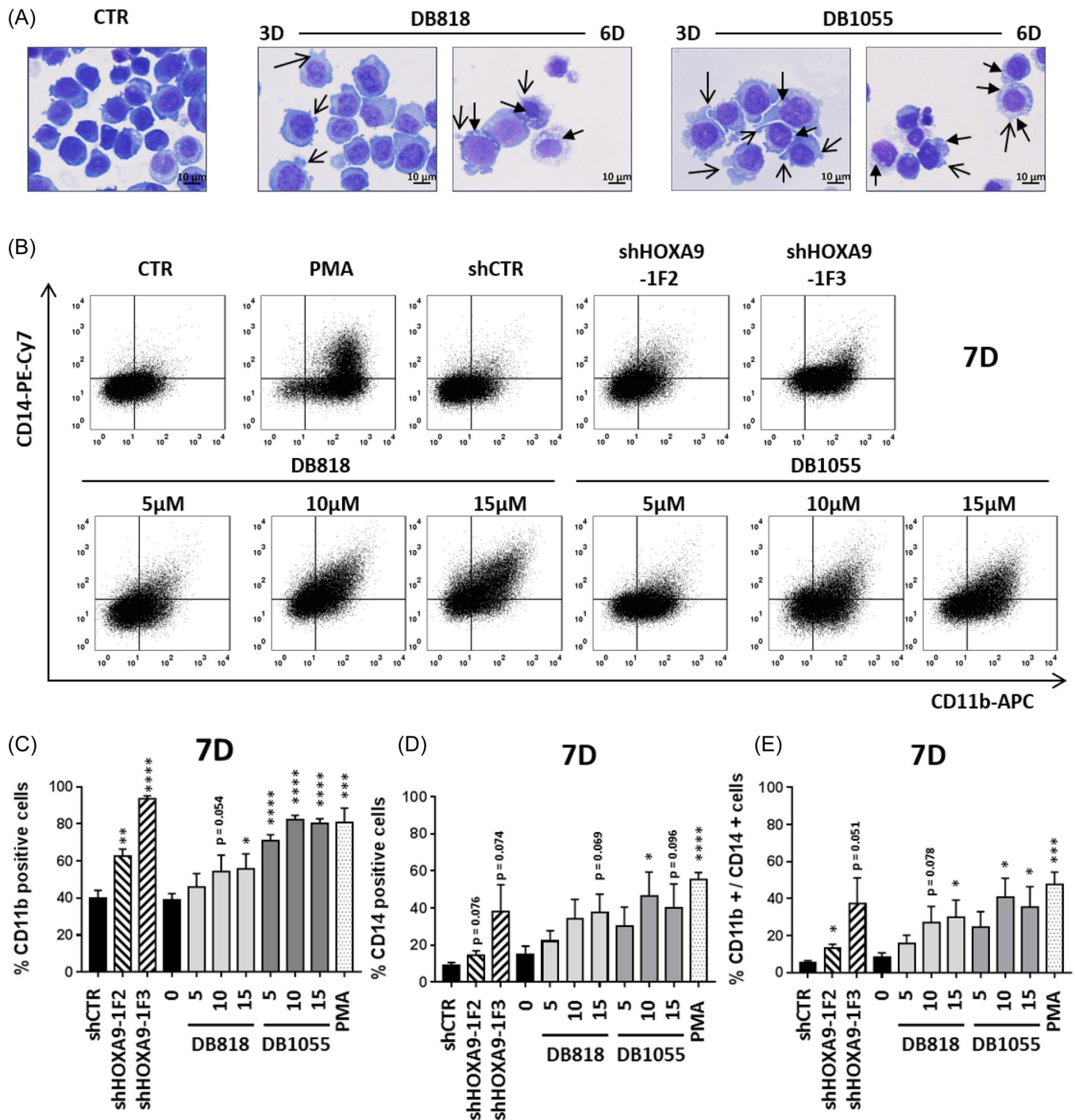


**FIGURE 2** Induction of cell differentiation. (A) Wright-Giemsa staining on cytocentrifuged preparations of THP-1 cells treated with 5  $\mu$ M of DB818 or DB1055 for 3 or 6 days. Open arrows point to cell membrane protrusions and solid arrows show accumulation of phagocytosis vesicles on representative images. (B) THP-1 cells were transduced with the different short hairpin RNA (shRNA) expressing lentiviruses or treated with DB818, DB1055, or PMA as a positive control (2.5 ng/mL) for 7 days prior to PI/CD11b-APC/CD14-PECy7 multiple labeling and flow cytometry analysis ( $n = 6$ ). Representative flow cytometry dot plots showing CD14-PECy7 over CD11b-APC expression levels derived from cells gated on PI-negative cells (DB818/DB1055/PMA) or PI-negative and GFP<sup>+</sup> cells for shRNA transduced cells as exemplified in Supporting Information S1: Figure S5a. (C–E) Quantification of CD11b and/or CD14-positive cells. Histograms represent the mean  $\pm$  SEM of the percentage of CD11b-positives (C), CD14-positives (D), or CD11b/CD14-double positive cells (E) in the live cell population (PI-negative) and GFP-positive cells when appropriated ( $n = 6$ ). Student t-test: \*\*\*\* $p < 0.0001$ ; \*\*\* $p < 0.001$ ; \*\* $p < 0.01$ ; \* $p < 0.05$ ;  $p$ -values between 0.05 and 0.1 are also specified above the corresponding bars.

shRNA with eGFP as a tracer in infection efficiency (93%–99% GFP-positive cells range for all experiments). Cell viability was assessed using CellTiter 96® Aqueous One Solution Cell Proliferation Assay kit (MTS, cell lines) or colorimetric diphenyltetrazolium bromide

(MTT, patient samples) according to the manufacturer's instructions. Clonogenicity was evaluated at 14 or 15 days on H4535 Human-Colony-Forming Cell Assays MethoCult® Enriched without EPO (Stemcell Technologies). Dishes were imaged using a DMi8 microscope



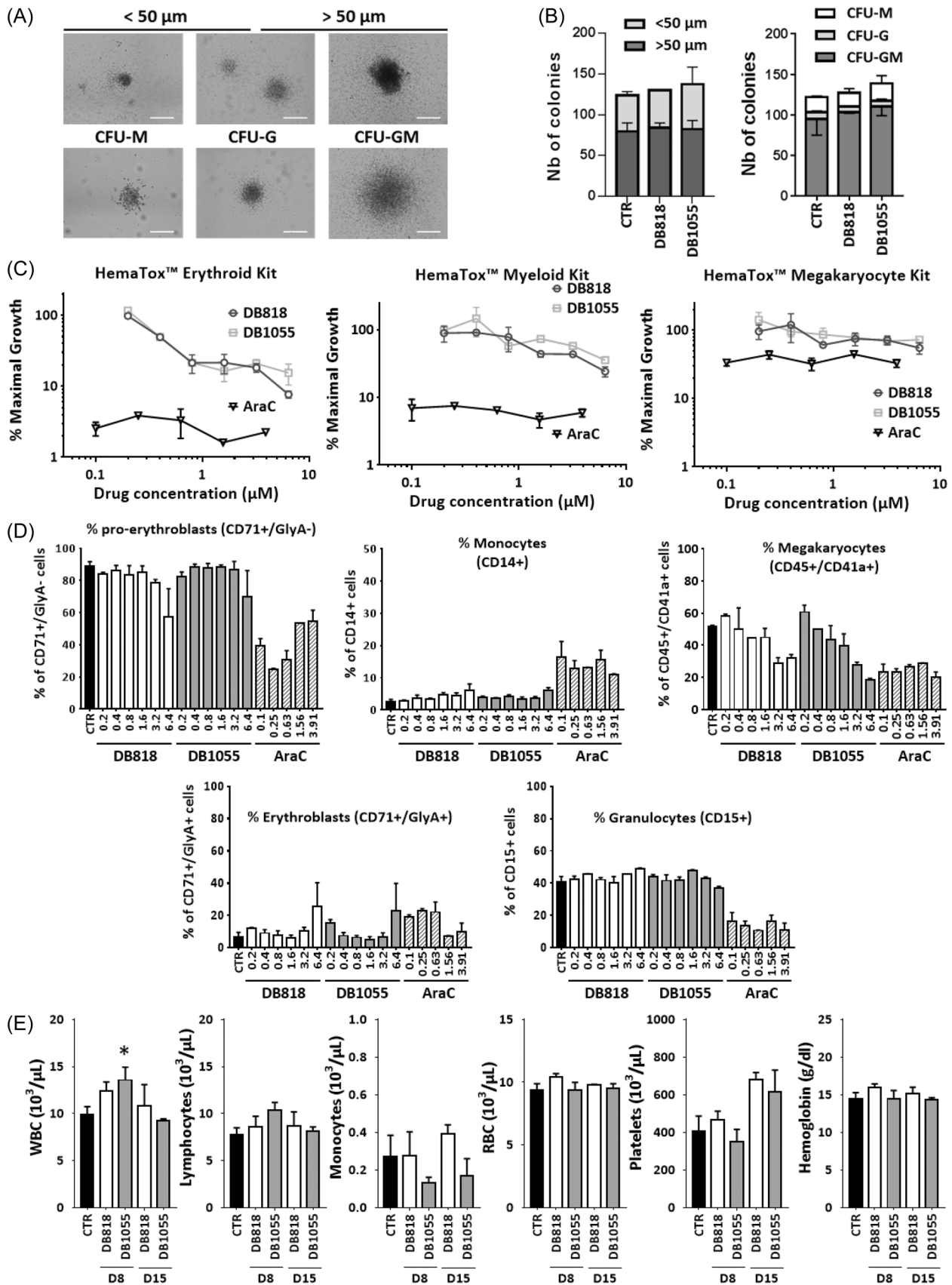


**FIGURE 3** (See caption on next page.)

**FIGURE 3** Evaluation of DB818 and DB1055 treatment on normal hematopoiesis. (A, B) Effect of DB818 or DB1055 treatment on colony-forming assays on normal human CD34<sup>+</sup> cells. Human CD34<sup>+</sup> cells (1000 cells) were seeded in duplicate with (or without) DB818 or DB1055 (2.5  $\mu$ M) for 15 days prior to quantification (A) regarding colony analysis for size (</>50  $\mu$ m) and subtypes (CFU-GM, CFU-G, and CFU-M) as determined on images (B) obtained using a DMi8 microscope ( $\times 5$  objective; Leica). White scale bars correspond to 50  $\mu$ m. Student *t*-test: \**p* < 0.05; otherwise nonspecific (*p* > 0.05). (C, D) Evaluation of lineage-specific toxicity of DB818 and DB1055 using HemaTox<sup>™</sup> erythroid, myeloid, and megakaryocyte kits. CD34<sup>+</sup> cells were induced for erythroid, myeloid, or megakaryocyte differentiation in the presence of DB818 (open circle), DB1055 (open square), or AraC (open triangle). Absolute cell count (C) was determined using Flow-Counts fluorospheres (Beckman Coulter) on an LSR-Fortessa<sup>™</sup>X-20 flow cytometer (BD Biosciences). Cell differentiation (D) was assessed by flow cytometry analyses. (E) In vivo hematological toxicity of DB818 and DB1055 in mice. C57BL/6jRj mice were treated with DB818 or DB1055 (30 mg/kg), or vehicle (CTR), on Days 1, 3, and 5. Blood samples were collected on Days 8 (D8, *n* = 4) and 15 (D15, *n* = 2) and analyzed for white (WBC) or red (RBC) cells blood count, lymphocytes, monocytes, or platelet count, as well as hemoglobin quantification using a veterinary hematology analyzer VetScan HM5. Student *t*-test: \**p* < 0.05; otherwise non-specific (*p* > 0.05).

(Leica). CFSE or Violet-CellTrace<sup>™</sup>-Cell-Proliferation Kits (Molecular Probes), and AnnexinV-APC cell staining or differentiation (monoclonal mouse anti-human CD14-PeCy7 and CD11b-APC antibodies or corresponding IgG1k isotypes; BD Pharmingen<sup>™</sup>) were used as described by manufacturers and analyzed on a CyAn-ADP flow cytometer, Beckman Coulter. For morphological change studies, cells treated to either 5  $\mu$ M of DB818 or DB1055 72 h were cytospun on a slide for 5 min at 800g using an EZ Single Cytofunnel<sup>™</sup> (Thermo Scientific). Subsequently, the cells were dried and stained using the Shandon<sup>™</sup> Kwik-Diff stain kit (Thermo Scientific), following the principles of classical Wright/Giemsa staining. Cells were photographed at  $\times 20$  magnification using an AxioScan Z1 (Zeiss) and analysis was conducted using the ZenBlue image software (Zeiss). Lineage-specific toxicity evaluated on CD34<sup>+</sup> cells is described in Supporting Information Methods.

## Gene expression and DNase-seq analyses

Total RNA samples were prepared using the RNeasy mini-kit (QIAGEN) according to the manufacturer's instructions and controlled for quality on the Agilent 2100 bioanalyzer (Agilent Technologies). One color whole Human (039494\_D\_F\_20150612 slides) 60-mer oligonucleotides 8 $\times$ 60k microarrays (SurePrint G3 Human GE v2 8 $\times$ 60K Microarray; Agilent Technologies) were used to analyze gene expression. cRNA labeling, hybridization, and detection were carried out according to the supplier's instructions (Agilent Technologies). For each microarray, cyanine 3-labeled cRNA was synthesized with the low-input QuickAmp labeling kit from 50 ng of total RNA. RNA Spike-In was added to all tubes and used as positive controls of labeling and amplification steps. The labeled cRNA was purified and 600 ng of each cRNA was then hybridized and washed following the manufacturer's instructions. Microarrays were scanned on an Agilent G2505C scanner and data were extracted using Agilent Feature Extraction Software<sup>®</sup> (FE version 10.7.3.1). Microarray data are available through the GEO depository from NCBI (accession no. GSE106831). All analyses were undertaken with Genespring software using a moderated *t*-test and False Discovery Rate (Benjamini-Hochberg) correction with a significant threshold at *p* = 0.05. Further investigations were carried out using Ingenuity Pathway Analysis<sup>®</sup> Software (IPA) and Gene Set Enrichment Analysis (GSEA, Desktop v3.0) and validated using qRT-PCR as described below. Ingenuity<sup>®</sup> Systems-6 software was used for pathway analysis based on differential gene expression. Significant pathways in IPA were identified using Fisher's exact test to score the highest *p*-values of deregulated cellular functions associated with |*Z*-score| > 1.65. GSEA software was used to highlight GO gene sets (biological processes, cellular components, molecular functions, oncogenic signatures, and curated gene sets) associated with whole genome expression lists derived from Genespring<sup>®</sup> software. Gene sets significantly enriched among the positive and negative correlating mRNAs were selected based on the GSEA FDR value (FDR < 0.05). RT-qPCR analysis is described in

the Supplementary Method and was performed using the primer sequences indicated in Supporting Information S1: Table 2. DNase-seq procedure is described in Supporting Information Methods.

## Patient samples

Studies using leukemia primary bone marrow and/or blood samples were approved by the Ethics Committee of the Institutional Review Board of the French Tumour Bank of Lille (Approval numbers CSTMT089/CSTMT0090) in accordance with the Declaration of Helsinki. The cytogenetic and molecular alterations were obtained using standard ISCN criteria as described<sup>2</sup> (Supporting Information S1: Table 3).

## In vivo experiments

All animal experiments, approved by the Lille animal ethics committee and notified to the French National Research Ministry, adhered to ethical standards with daily observation in accordance with European rules. For in vivo hematologic toxicity evaluation, C57BL/6jRj mice (Envigo) were treated 1 week (Days 1, 3, and 5) with DB818 and DB1055 administered intraperitoneally (i.p.) at 30 mg/kg or with the vehicle. On Days 8 and 15, blood was collected by submandibular puncture in ethylenediaminetetraacetic acid-coated microtubes, and a complete blood count was performed using the veterinary hematology analyzer VetScan HM5 (Abaxis). For shHOXA9 investigations, THP-1-Luc cells were generated using a lentivirus expressing the luciferase (luciferase cDNA-IRES-puromycin resistant cDNA) to generate a clone. THP-1-Luc or wild-type THP-1 cells were transduced for 24 h with lentiviruses that express different shRNAs (shHOXA9-1F2/-1F3 or shCTR) prior to being washed six to eight times and then i.p. injected in 6-8-week-old NOD.Cg-Prkdc<sup>scid</sup>-Il2rg<sup>tm1Wjl</sup>/SzJ (NSG) mice (1  $\times$  10<sup>6</sup> THP-1-Luc clone cells for leukemia burden follow or 2  $\times$  10<sup>6</sup> wild-type THP-1 cells for global mice survival analysis, *n* = 5-6 per group) for an efficiency of transduction >99% of GFP-positive cells in all conditions. For luciferase quantification, leukemic cell dissemination was monitored on both the ventral and the dorsal views at 2, 14, 28, and 40 days postcell injection. Images were collected 10-15 min after i.p. injection with luciferin (150 mg/kg; PerkinElmer) using the IVIS50<sup>®</sup> imaging system (PerkinElmer). Quantification by FACS of GFP-positive cells (FITC) specific for shRNA-expressing lentivirus-infected cells within the pool of total hCD45-positive (THP-1) cells was performed in spleen cells isolated from mice at end-point sacrifice. For antileukemic activities of DB1055 and DB818, NSG mice were i.p. injected with THP-1, U937, or EOL-1 cells as indicated in the legends of figures. DB1055 was i.p. administered at 20 mg/kg (THP-1) or 40 mg/kg (PDX), DB818 at 5 mg/kg, and cytarabine (AraC) at 100 mg/kg as indicated in figures and legends. At sacrifice, bone marrow (flushed from the two femurs), intra-cardiac blood, spleen, and potential peritoneal ascites were collected in a sterile

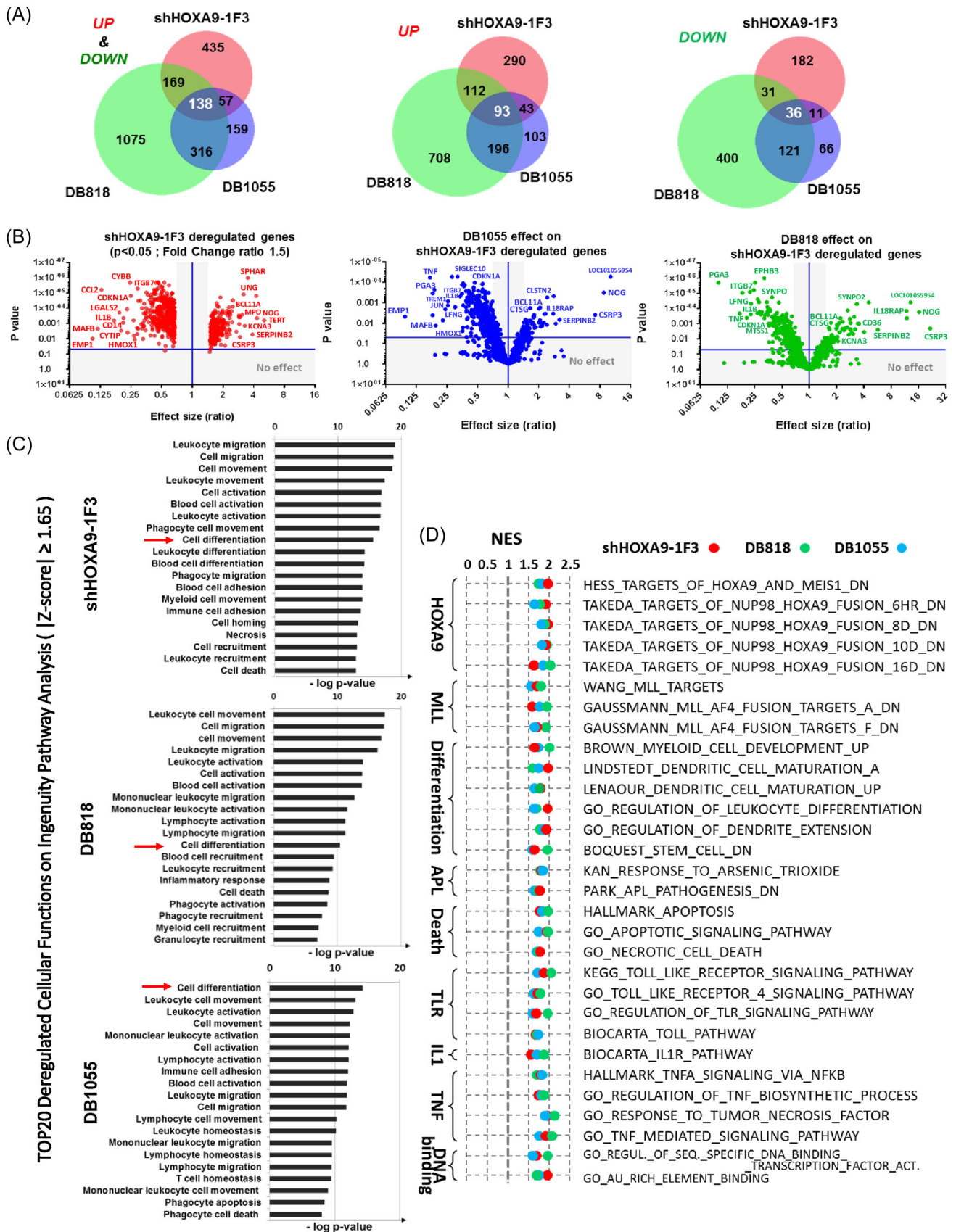


**FIGURE 4** (See caption on next page).



**FIGURE 4** Identification of commonly deregulated genes and processes using transcriptomic analysis in THP-1 cell model. Gene expression profile was obtained in quadruplicate for THP-1 cells invalidated for HOXA9 (shHOXA9-1F3) versus control (shCTR) for 48 h or THP-1 cells treated or not using DB818 or DB1055 for 24 h. (A) Venn diagrams for the intersection of genes being statistically significant ( $p < 0.05$ ) and differently expressed in each condition (relative to the corresponding control) with (top Venn diagram, UP&DOWN, fold change (FC)  $> 1.5$  or  $< -1.5$ ), statistically significant upregulated (middle Venn diagram, UP, FC  $> 1.5$ ), and statistically significant downregulated (bottom Venn diagram, DOWN, FC  $< -1.5$ ). (B) Volcano plots for all deregulated genes in shHOXA9-1F3 transduced cells (top plot) or from DB1055 (middle plot) or DB818 (bottom plot) gene expression effect within the shHOXA9-1F3 deregulated gene list. (C) Top 20 of the deregulated cellular networks identified by ingenuity pathway analysis (IPA) with significant  $|z\text{-score}|$  of at least 1.65 and ordered on the top  $-\log p$ -values highlights the implication of differentiation, cell death leukocyte activation, and migration/movement processes. (D) Gene Set Enrichment Analysis (GSEA) assays highlight commonly deregulated processes and correlate with HOXA9 and MLL-associated curated gene set terms. NES values are plotted for each GSEA from shHOXA9-1F3, DB1055, or DB818 deregulated gene sets (GSEA version 6.2). Corresponding GSEA plots with NES,  $p$ -values, and Venn diagrams are presented in Supporting Information S1: Figures S6 and S7 together with other related GSEA-CGP results.

environment. Organs were weighted and measured. Splenic cells were dissociated in phosphate-buffered saline buffer. Flow cytometry analyzed human leukemic cells for GFP expression (shRNAs) and/or hCD11b- and/or hCD45-labeling in the blood, spleen, bone marrow, and ascites. Human cells were identified from mouse cells using monoclonal mouse anti-human antibody CD45-APC  $\pm$  hCD11b-PE-Cy5 or corresponding isotypes (IgG1k; eBioscience) for detection of THP-1 and PDX cell dissemination. Single-cell suspensions were analyzed by flow cytometry (CyAn ADP; Beckman Coulter) as described above. Two patient-derived xenografts (PDX) were obtained by intratibial injection of  $2 \times 10^6$  hCD45-positive cells isolated from the spleen of recipient mice used for patient blast amplification. After 4 weeks of implantation (~1%–3% blasts evidenced by FACS from mice blood sampling using anti-hCD45 antibody), mice were treated with DB1055 or AraC for 3 (PDX-1) or 4 (PDX-2) series of treatments, each corresponding to 1 week of treatment on Days 1, 3, and 5 followed by 2 weeks OFF (without treatment). Mice were sacrificed after the last week of treatment (PDX-1) or after 1 week OFF following the last week of treatment (PDX-2) based on ethical protocol.

## Statistics

All statistical analyses, excluding transcriptomic differential gene expression described in Supporting Information Methods, were determined with Prism7/GraphPad Software using Student two-sided unpaired  $t$ -tests or log-rank (Mantel–Cox) test (Kaplan–Meier survival curves).

## RESULTS

DB1055 and DB818 (Figure 1A,B) were initially chosen for their robust interaction with the HOXA9-cognate sequence and their effective competition for HOXA9 binding to DNA.<sup>21</sup> In this study, we extended our assessment of their activities to human AML cell lines and blasts obtained from patients. We evaluated their impact on various cellular aspects, including cell death and differentiation, conducted analyses on gene regulation and pathways, assessed efficacy on primary cultures, and validated the *in vivo* antileukemic potential on both AML cell lines and patient-derived xenografts.

### DB1055 and DB818 affect the survival of HOXA9-positive human AML cell lines

We examined the impact of DB1055 and DB818 on cell survival ( $IC_{50}$ ) across fourteen distinct human AML cell lines with diverse FAB/cytogenetic/molecular characteristics. Notably THP-1 (MLL-AF9), U937 (CALM-AF10 fusion), EOL-1 (MLL-PTD mutation), and OCI-AML3 (NPM1c+ mutation) exhibited a strong correlation with

HOXA9 expression (Figure 1A,B) and were therefore included for subsequent evaluation. The cellular effects of DB1055 or DB818 were investigated in comparison with HOXA9 knockdown using efficient lentivirally-transduced shHOXA9. The efficiency of transduction was assessed by flow cytometry, evaluating GFP expression (Supporting Information S1: Figure 1a). Concurrently, knockdown efficiency was gauged through qRT-PCR (Supporting Information S1: Figure 1b) and validated by western blot analysis (Supporting Information S1: Figure 1c,d). Notably, these assessments align with previously published results that utilized the same shRNA sequences, ensuring consistency in the experimental approach.<sup>26</sup> The THP-1 cell model, chosen for its ability to form colonies and differentiate in macrophage-like cells,<sup>30</sup> provided an appropriate model for studying antiproliferative activity, cell death, and differentiation. Both shRNA knockdown and functional HOXA9 inhibition by DB1055 or DB818 led to reduced cell growth kinetics (Supporting Information S1: Figure 2a). Such slowdowns were associated with decreased cell proliferation (Figure 1C), reduced colony formation (Figure 1D), and induction of cell death, evidenced by an increase in propidium iodide (PI)-positive cells (Figure 1E and Supporting Information S1: Figure 2b in comparison with AraC treatment Supporting Information S1: Figure 2c). An increase in apoptosis was also observed using DB1055 and DB818, as indicated by AnnexinV/PI-double positive staining (Figure 1D for 7 days and Supporting Information S1: Figure S2d at 3 days posttreatment or transduction). We extended the evaluation to U937 and EOL-1 cell lines (Figure 1A,B) to validate these findings (Supporting Information S1: Figure 3). Particularly, DB1055 and DB818 significantly decreased the number and size of colonies in HOXA9-positive U937, EOL-1, MV4-11, and SHI-1 cell lines (Supporting Information S1: Figure 4a-d) while HOXA9-independent leukemia cells remained unaffected (Supporting Information S1: Figure 4e).

Therefore, our comprehensive evaluation of DB1055 and DB818 revealed their significant impact on cell survival in strong correlations with HOXA9 expression in specific AML cell lines like THP-1, U937, and EOL-1. Furthermore, the consistent demonstration of antiproliferative, proapoptotic effects of DB1055 and DB818 across various AML cell lines underscores their potential as targeted therapeutic agents in HOXA9-dependent AML subtypes.

### DB1055 and DB818 induce monocyte-to-macrophage differentiation features

Treatment of THP-1 cells with DB818 or DB1055 induced morphological changes indicative of differentiation, including a reduced nucleus-to-cytoplasm ratio, basophilic cells, and the presence of both phagocytic vacuoles and pseudopods (Figure 2A). Furthermore, DB1055- or DB818-treated THP-1 cells were compared to

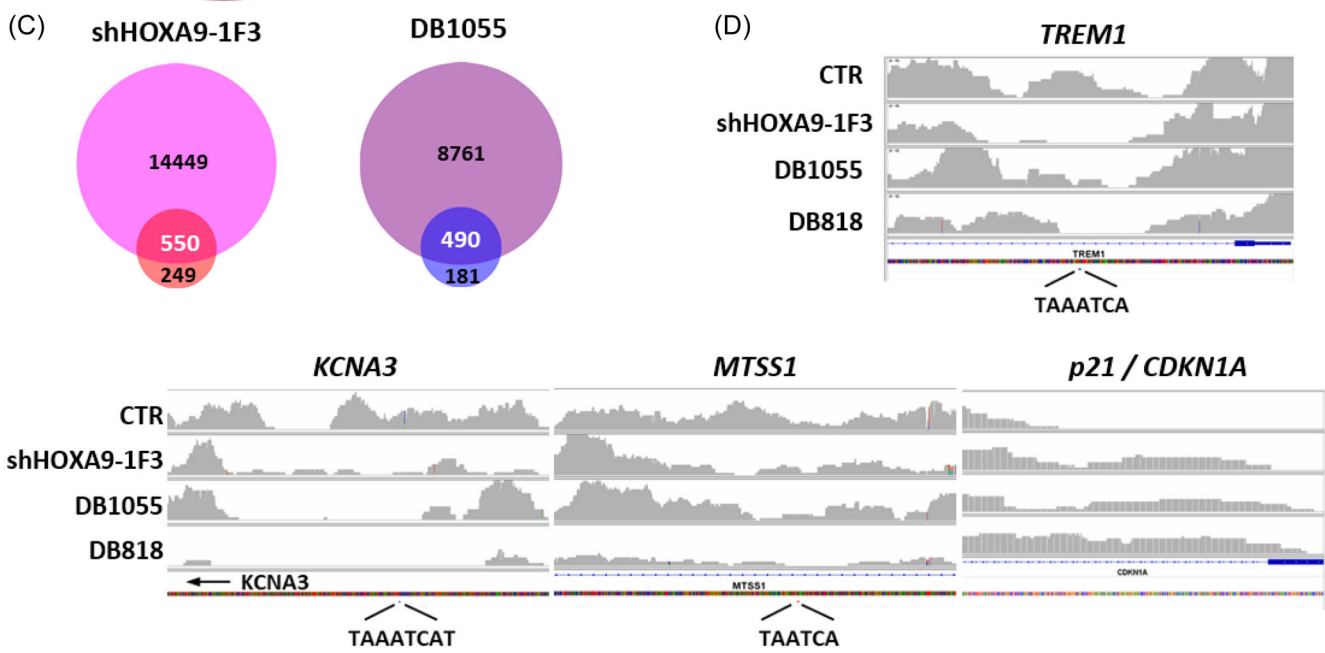
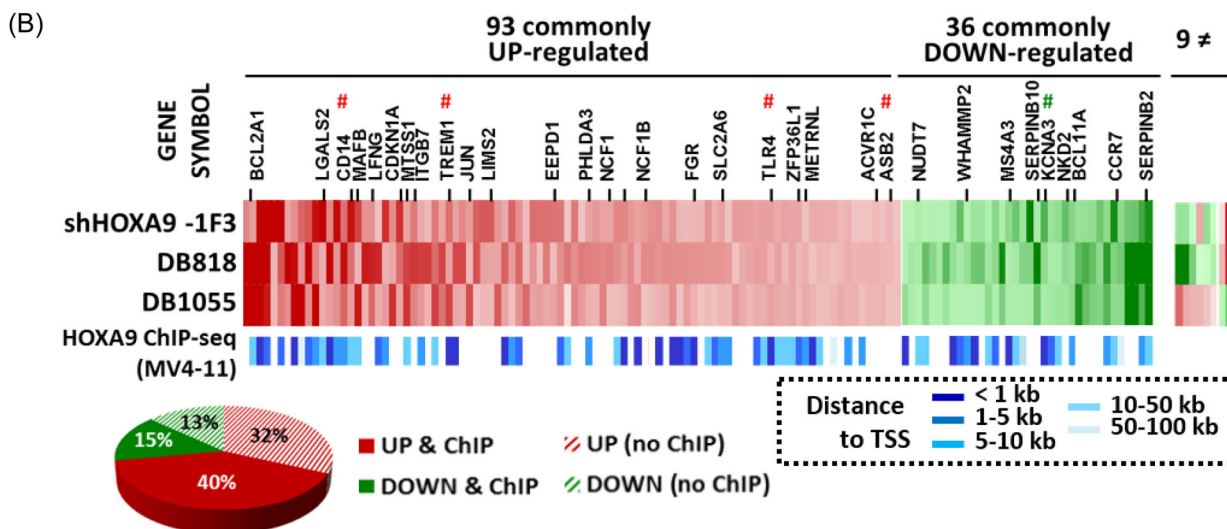
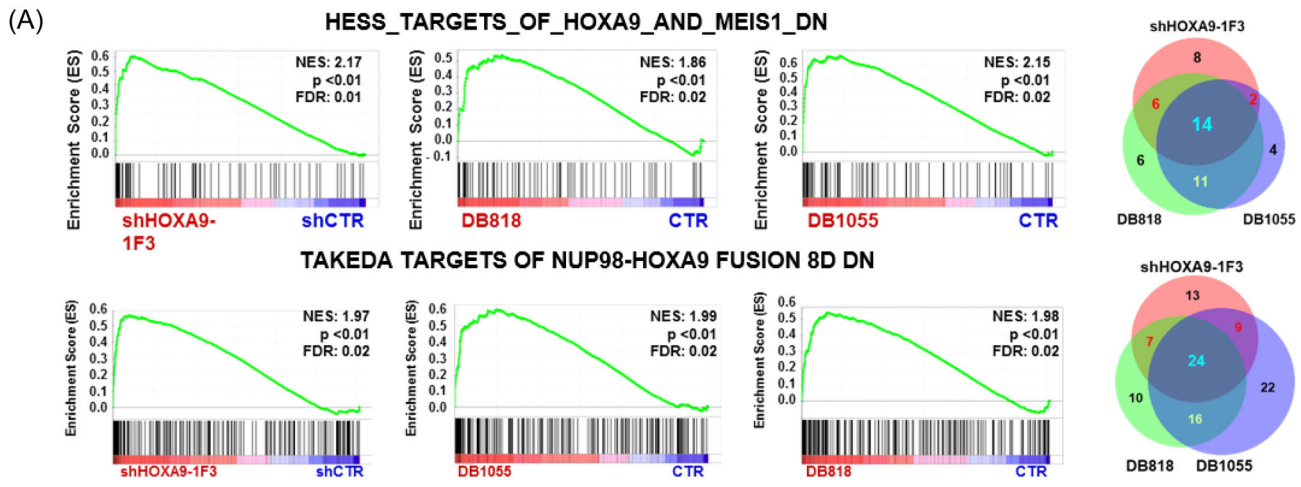


**FIGURE 5** (See caption on next page).

**FIGURE 5** Comparison of DB1055 and DB818 deregulated genes with ChIP-seq and DNase-seq data. (A) “HESS TARGETS OF HOXA9 AND MEIS1 DN” and “TAKEDA TARGETS OF NUP98-HOXA9 FUSION 8D DN” curated gene sets terms (C2, CGP: chemical and genetic perturbations) highlighted from GSEA for both shHOXA9 and DB818 or DB1055 cell treatment. The normalized enrichment scores (NES), nominal *p*-values, and FDR are shown in each caption. Corresponding Venn diagrams are presented on the right of the panel and a heatmap for implicated genes is given in Supporting Information S1: Figure 8. (B) Heatmap for the expression change of the 138 genes commonly significantly deregulated in the three conditions (HOXA9 inactivation and treatment with DB818 or DB1055) and position of different genes of interest and identification of the presence of a peak from HOXA9 ChIP in MV4-11 cells.<sup>32</sup> The intensity of the blue color depends on the distance to TSS as defined in the figure. In white: genes in which the distance to TSS was over 100 kb. Circular diagram represents the percentage of the 138 commonly dysregulated genes (UP or DOWN) that present (plain color) or not (dashed color) a ChIP-peak identified for HOXA9 binding in the MV4-11 cell line. (C) Venn diagrams for comparison of the lists of deregulated genes from transcriptomic analyses and genes identified at the proximity of differential peaks from global DNase-seq analyses as depicted in the Supporting Information Material and Methods section. (D) IGV visualization of some peaks attributed to some of the genes differentially expressed in panel b (arrows). Potential HOXA9 binding sites (based on aTGATT(T)A/TAA(A)TCat sequence as a HOX/PBX consensus site) are highlighted for TREM1, KCNA3, and MTSS1 and the sequences indicated, whereas no such potential site is present at the increased peak for CDKN1A.

PMA-differentiated THP-1 cells<sup>30</sup> for CD11b and CD14 cell surface differentiation markers quantified by flow cytometry (Figure 2B). A substantial increase in CD11b cell surface expression was observed 7 days posttreatment (Figure 2B), starting on Day 2 (DB818/DB1055) or Day 3 (shHOXA9) (Supporting Information S1: Figure 5a,b). CD14 expression increased later at Day 4 post-DB818/1055 treatment and even more prolonged elevation with shHOXA9-1F2 or -1F3 transduction, occurring on Day 7 (Figure 2B and Supporting Information S1: Figure 5a,b). Moreover, the proportion of CD11b/CD14 double-positive cells, characterizing monocytic to macrophage differentiation, increased with DB1055 and DB818 treatments in a dose-dependent manner and similarly to shHOXA9 (Figure 2E and Supporting Information S1: Figure 5b) but not after AraC treatment (Supporting Information S1: Figure 5c). These results demonstrate that DB818 and DB1055 counteract differentiation blockade to restore monocytic-to-macrophage differentiation. Differentiation was also induced in EOL-1 and U937 treated with DB1055 or DB818 (Supporting Information S1: Figure 6).

In brief, treatment with DB818 or DB1055 induced phenotypic changes indicative of monocytic-to-macrophage differentiation in THP-1 cells, accompanied by comparable effects in EOL-1 and U937 cells.

### DB1055 and DB818 exhibit no adverse effects on normal hematopoietic cell survival and the differentiation process

Considering the involvement of HOXA9 in maintaining normal hematopoietic progenitor cell maintenance and its role in differentiation blockade,<sup>31</sup> we evaluated the impact of DB818 and DB1055 on normal hematopoiesis. Treatment of human bone marrow CD34<sup>+</sup> (hCD34<sup>+</sup>) cells with DB818 or DB1055 showed no statistically significant changes in the total number, size, or type of CFU-M/-G/-GM colonies (Figure 3A,B). Treatment was performed at 2.5  $\mu$ M to compare with the reduction of colonies observed in similar conditions on THP-1 cells leading to a 40%-50% decrease in the numbers of colonies, and with other AML or non-AML cell lines (Supporting Information S1: Figure 4). In addition, it was observed that both DB1055 and DB818 exhibited significantly lower levels of toxicity compared to AraC toward the myeloid/megakaryocyte/erythroid sub-populations (Figure 3C). Furthermore, these inhibitors did not promote the differentiation of normal hCD34<sup>+</sup> cells into monocytes, granulocytes, megakaryocytes, or erythroblasts (Figure 3D). Ultimately, the administration of DB818 or DB1055 to C57BL/6 mice did not result in a significant decrease in white or red blood cell counts (Figure 3E). Collectively, these experiments show that targeting HOXA9 with our inhibitors does not hinder normal hematopoiesis.

### Transcriptomic analysis of DB818, DB1055, and shHOXA9 treatments unveils frequently deregulated genes

Gene expression profiling was used to characterize common changes occurring after HOXA9 knockdown or functional inhibition by DB818 or DB1055 in the THP-1 model (Figure 4). Nearly 138 genes were found commonly deregulated by DB818, DB1055, and shHOXA9-1F3 (fold change >1.5, Figure 4A). The distribution of genes deregulated upon HOXA9 knockdown with DB1055 and DB818 transcriptome is presented as volcano plots in Figure 4B, illustrating fold change relative to *p*-values. The top 20 most deregulated Ingenuity Pathway Analysis (IPA) functions were associated with cell processes related to differentiation, activation, movement/migration, and death in all three conditions (Figure 4C). Furthermore, Gene Set Enrichment Analysis (GSEA) analysis confirmed that shHOXA9 transcriptomic signature for THP-1 aligns with previously published data related to GSEA oncogenic signatures and curated gene sets involving the deregulation of HOXA9 expression, MLL, differentiation, cell death, and DNA binding, among others. These items were consistently highlighted in GSEA from DB1055 and DB818 cell treatment with Normalized Enrichment Score (NES) values over 1.5 (Figure 4D and Supporting Information S1: Figures 7-8).

### Evidence for HOXA9 target inhibition at the DNA binding level

GSEA analysis (Figure 4D) underscored the significance of the CGP (C2 chemical and genetic perturbations) curated gene sets, specifically “HESS TARGETS OF HOXA9 AND MEIS1 DN” and “TAKEDA TARGETS OF NUP98-HOXA9 FUSION 8D DN” in both shHOXA9 and DB818 or DB1055 cell treatments. A substantial proportion of genes commonly deregulated, with an absolute fold change exceeding 1.5, was identified in the Venn diagrams and is visually represented in the corresponding heatmaps and tables (Figure 5A, Supporting Information S1: Figure 9 and Supporting Information S1: Table S4). We further investigated common features at the HOXA9 target level from the 138 commonly deregulated genes corresponding to 93 commonly upregulated and 36 commonly downregulated genes (Figure 4A). Only nine genes displayed inconsistent regulation (Figure 5B). Because of the lack of ChIP-seq grade and reliable anti-HOXA9 antibodies,<sup>33</sup> and since it has been shown that distinct MLL fusions can induce HOXA9 overexpression, we compared our list of deregulated genes after treatment with DB818/DB1055 of THP-1 cells (MLL-AF9 fusion) with genes with HOXA9 binding sites identified by ChIP-seq analyses in MV4-11 cells (MLL-AF4 fusion).<sup>34</sup> Despite THP-1 and MV4-11 cell lines present distinct MLL fusions (MLL-AF9 and MLL-AF4, respectively), both MLL-fused proteins have

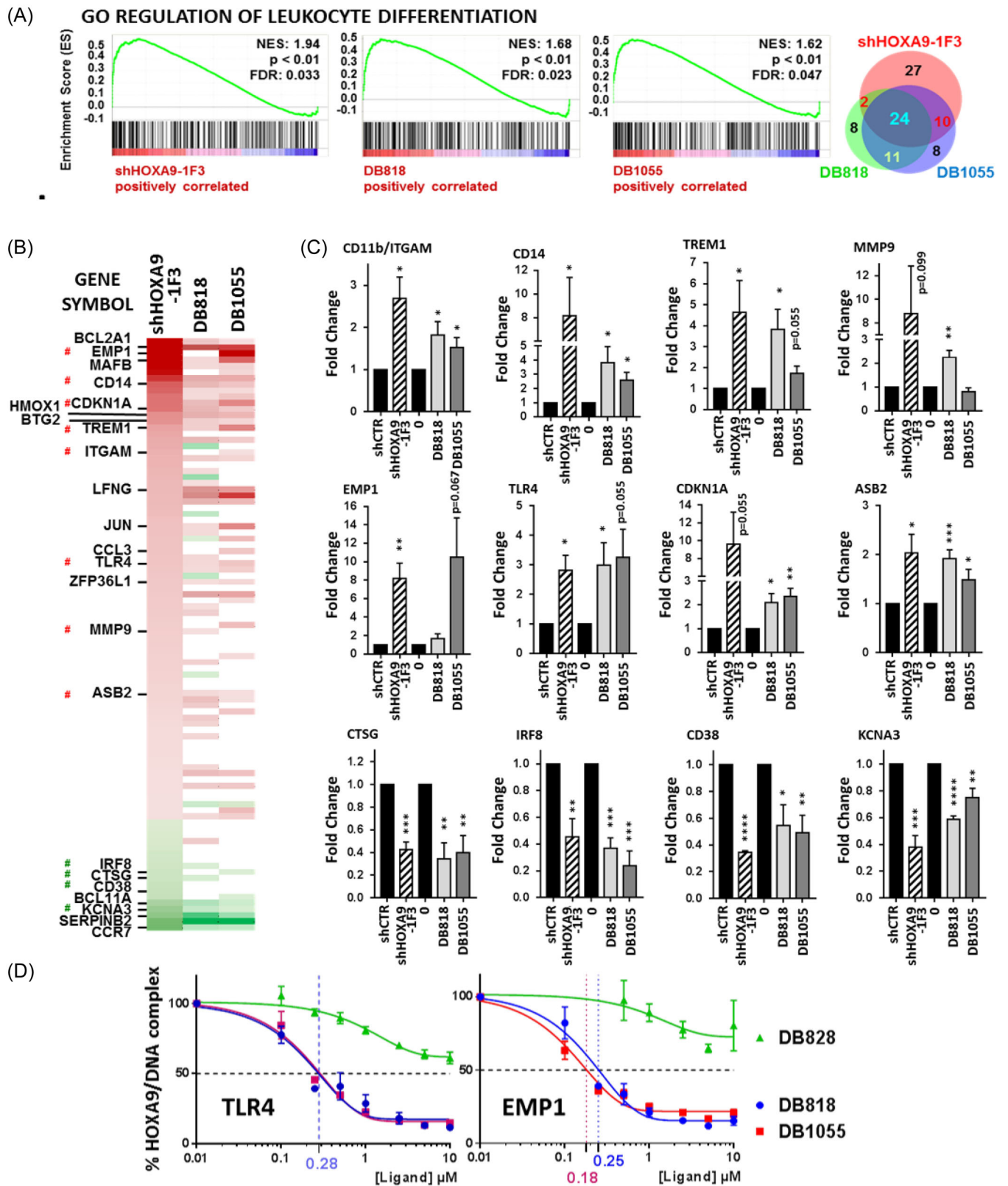


FIGURE 6 (See caption on next page).



**FIGURE 6** Global gene deregulation analysis identified common activation of differentiation process upon shHOXA9 as well as DB818 or DB1055 treatment of THP-1. (A) Gene Set Enrichment Analysis assays for GO term “regulation of leukocyte differentiation” for both HOXA9 invalidation and cell treatment with DB818/1055. The normalized enrichment scores (NES), nominal *p*-values, and FDR are shown in each caption and the corresponding Venn diagram is presented on the right panel. (B) Heatmap for the expression of genes associated with the “cell differentiation” item from Ingenuity Pathway Analysis (localized by a red arrow in Figure 3B) ranked on the expression from shHOXA9-1F3 gene list. #, genes of interest further validated using quantitative reverse transcription polymerase chain reaction (qRT-PCR). (C) Validation of gene expression deregulation by qRT-PCR for a series of deregulated genes identified in (C) (four to eight independent experiments). Corresponding significant statistics (Student *t*-test) are calculated relatively to the corresponding control (CTR for DB818 or DB1055 treatments and shCTR for shHOXA9-1F3) and indicated on the graphs: \*\*\*\**p* < 0.0001; \*\*\**p* < 0.001; \*\**p* < 0.01; \**p* < 0.05; or as specified on graphs. (D) Enzyme-linked immunosorbent assay-derived DNA binding inhibition assay. Double-stranded oligonucleotides containing the HOXA9 putative binding site at EMP1 and TLR4 gene promoters identified from MV4-11 ChIP-peaks<sup>34</sup> were evaluated with human HOXA9 protein expressed from reticulocyte lysate in the presence of increasing concentrations of DB818 or DB1055 (*n* = 4–6) as described.<sup>21</sup> The unselective DB828 compound was used as a control. The concentrations of DB818 and DB1055 that inhibit 50% of the HOXA9/DNA complex are indicated in the graph.

been described to control HOXA9 expression. Approximately 55% of genes in the heatmap showed at least one ChIP-seq peak for HOXA9 in the MV4-11 cell context, depicted in the bottom line in blue colors (Figure 5B). To offer a more comprehensive understanding of the gain/loss of transcriptional complexes across the entire chromatin following DB1055 and DB818 treatment, we conducted DNase I hypersensitive site sequencing (DNase-seq) analyses in THP-1 cells. While 60–70 million reads were obtained for both DB1055 treatment, shHOXA9 transduction, and controls, only 30 million reads were obtained using DB818-treated THP-1 cells. Quantitative analyses were performed for DB1055 and shHOXA9 samples (Supporting Information S1: Figure 10). The list of genes closest to the identified variable peaks was compared with the list of genes significantly modified under the same treatment (Figure 5C). Around 68% and 73% of the deregulated genes were identified in the DNase-seq analysis for shHOXA9-1F3 and DB1055 treatment, respectively. Illustrations of modified DNase-seq peaks are presented in Figure 5D for *TREM1*, *KCNA3*, *MTSS1*, and *CDKN1A*, among others (Supporting Information S1: Figure 11). Moreover, some DNase-seq modified peaks coincided with ChIP-seq peaks identified by Zhong et al.<sup>34</sup> (Supporting Information S1: Figure 10). Some of them contained the HOXA9/PBX consensus binding sites 5'-aTGATT(T)A/5'-TAA(A)TCAT, as indicated in the different panels (Figure 5D and Supporting Information S1: Figures 10 and 11).

In brief, our comprehensive analysis of gene expression changes, HOXA9 targets, and chromatin modifications, including ChIP-seq and DNase-seq analyses in response to DB1055 and DB818 treatment, revealed consistent deregulation of genes associated with critical AML-related functions and identified potential transcriptional complexes.

### Inhibiting HOXA9 alters the expression of genes associated with macrophage differentiation

Common features associated with differentiation were consistently identified through GSEA and IPA analyses (Figure 4C,D). Notably, the “GO-Regulation of leukocyte differentiation” geneset (Figure 6A) revealed a substantial number of genes commonly up- or down-deregulated between the DB818/DB1055/shHOXA9 conditions as depicted in the Venn diagram. The “Cell differentiation” item from IPA (Figure 6B), further emphasized these findings, with some genes validated through qRT-PCR. Among them, some are upregulated as attempted during the differentiation process (among which *CD11b/ITGAM* and *CD14*,<sup>30</sup> *TLR4*, *TREM1*, *EMP1*, *CDKN1A*...) whereas others are downregulated in the course of differentiation (*KCNA3*, *CTSG*, *IRF8*, or *CD38*) (Figure 6C and Supporting Information S1: Table S5). Two of the HOXA9 ChIP-seq peaks identified by Zhong et al.<sup>34</sup> were found within *TLR4* and *EMP1* genes (peaks chr9-5 and chr12-1340,

respectively) (Supporting Information S1: Figure 10). ELISA-derived DNA binding assays showed that both DB818 and DB1055 inhibited HOXA9 binding to *TLR4* and *EMP1* target sequences with an IC<sub>50</sub> of 0.2–0.3 μM, whereas DB828, previously identified as an inactive compound,<sup>21</sup> did not (Figure 6D).

### HOXA9 expression is essential for THP-1 leukemia burden in vivo mouse model

We then validated the antileukemic activity in vivo by confirming the leukemic role of HOXA9 using luciferase-expressing THP-1 cells transduced with lentiviruses encoding shCTR, shHOXA9-1F2, or shHOXA9-1F3, tracking leukemia burden through in vivo bioluminescence imaging in immunodeficient NSG mice. Longitudinal in vivo imaging revealed a significant reduction in total body luminescence with shHOXA9-1F2/1F3 compared to shCTR-expressing cells (Figure 7A,B, Supporting Information S1: Figure 12a,b), associated with reduced splenomegaly at day 40, particularly for the most efficient shHOXA9-1F3 (Figure 7C). A similar effect was observed in a previously published study using the shHOXA9-1F3 sequence against t(4;11) SEMK2 B-ALL cell model inoculated in NSG mice.<sup>31</sup> Despite efficient transduction (revealed 48 h post-infection) with ~95%–99% of THP-1 cells at injection, most of the THP-1 (hCD45-positive) cells recovered from spleens at sacrifice in shHOXA9-transduced sub-groups were GFP-negative, suggesting that HOXA9-knockdown THP-1 cells underwent cell death, while non-transduced (GFP-negative) cells proliferated and were ultimately responsible for mice death (Figure 7D), in correlation with the absence of significant differences in total hCD45-positive cells (either GFP-positive and -negative) in the spleen, bone marrow, liver, and blood at sacrifice (data not shown). In a second series of mice engrafted with transduced-THP-1 cells, the median survival was extended to 55 and 66 days for shHOXA9-1F2 and -1F3, respectively, compared to 48 days for shCTR (Figure 7E). Thus, the THP-1 leukemia model is validated as a HOXA9-dependent AML model suitable for in vivo evaluation of our inhibitors.

### DB1055 and DB818 show antileukemic activities in AML cell lines in vivo mouse model

The effects of the HOXA9/DNA binding inhibitors were first evaluated in a wild-type THP-1 in vivo model. In the wild-type THP-1 in vivo model, the treatment schedules were based on mice tolerance, with DB1055 being better tolerated by i.p. injection than DB818 and used at a higher concentration. DB1055 did not impact animal body weight (Supporting Information S1: Figure 12d). DB1055 in vivo evaluation was performed according to the treatment schedule

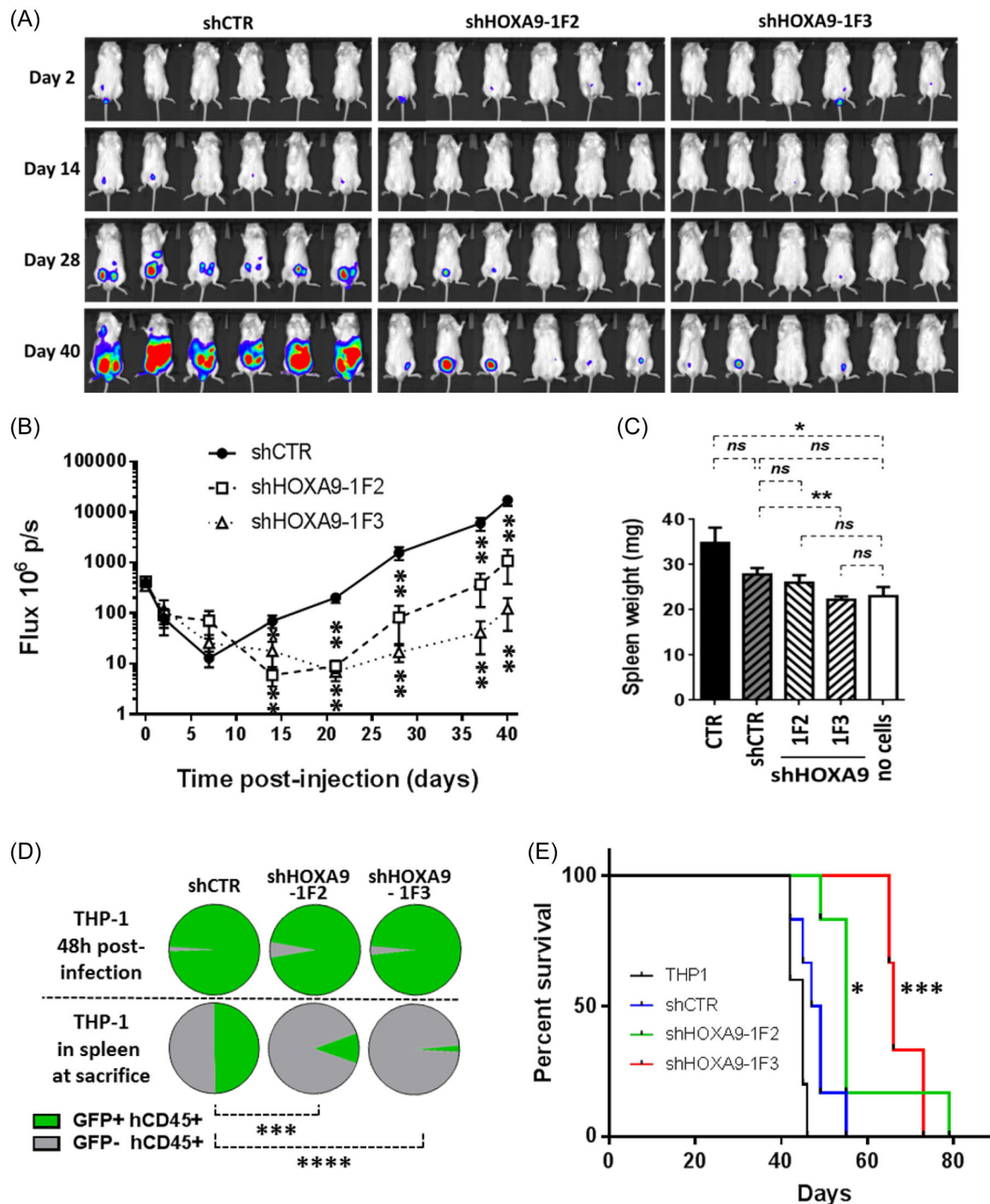


**FIGURE 7** In vivo validation of THP1 as an HOXA9-dependant mice cell model. (A) Representative images for bioluminescence kinetic analyses after i.p. inoculation in NSG mice ( $n = 6$  per group) of THP1-Luc cells ( $1 \times 10^6$ ) that were previously transduced by short hairpin RNA (shRNA)-expressing lentiviruses. (B) Quantification of the time course for bioluminescent THP1-Luc responses to HOXA9 invalidation. Quantification is expressed in photons/second over time (in days). (C) Spleen weight of mice from euthanized altogether on Day 41. Results are presented as mean  $\pm$  SEM. Statistics, Student *t*-test: \*\*\*\* $p < 0.0001$ ; \*\*\* $p < 0.001$ ; \*\* $p < 0.01$ ; \* $p < 0.05$ ; ns, nonspecific or *p*-values as indicated in graphs. (D) Quantification by flow cytometry of GFP status of THP1 (hCD45-positive) cells at 48 h after lentiviral infection or in spleen isolated from mice at end-point sacrifice. (E) Kaplan-Meier plot for mice survival upon HOXA9 invalidation. THP1-Luc (WT) cells ( $2 \times 10^6$  cells) were transduced or not with shRNAs (WT THP-1, black line,  $n = 5$ ; shCTR, blue line,  $n = 6$ ; shHOXA9-1F2, green line,  $n = 6$ ; and shHOXA9-1F3, red line,  $n = 6$ ) 24 h before engraftment. Statistics were performed using log-rank analysis of the Kaplan-Meier survival curve.

presented in Figure 8A. DB1055 significantly decreased THP1-induced splenomegaly (Figure 8B,C) whereas Ara-C treatment did not affect spleen size, indicating THP1 as an Ara-C-chemoresistant model. The differentiation of THP1 cells in mice was evaluated at

sacrifice, revealing a significant increase in hCD11b-positive human THP1 cells in DB1055-treated mice for compartments associated with more differentiated cells, such as blood and peritoneal ascites, but not in the bone marrow and spleen (Figure 8C). DB818 was then

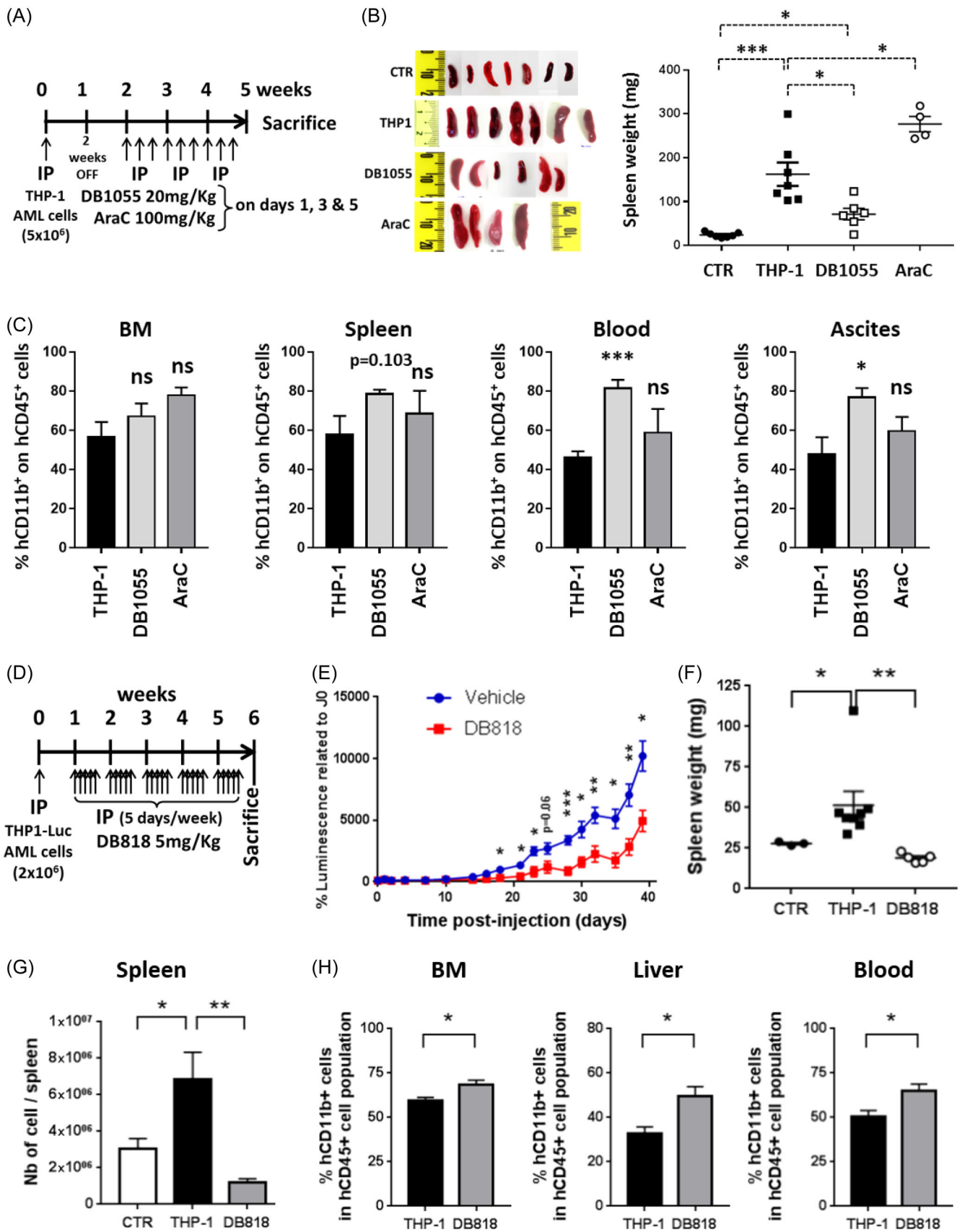


**FIGURE 8** (See caption on next page).

**FIGURE 8** In vivo validation of DB1055 and DB818 antileukemic and differentiation activities in THP-1 grafted mice model. (A) Schedule of DB1055 and AraC treatment of 5 million THP-1 engrafted NSG mice. IP, intraperitoneal injection. (B) Photographs and weight graph of spleens showing reduced splenomegaly upon DB1055 treatment. (C) Flow cytometry analysis of the percentage of human CD11b-positive cells upon THP-1 cells (identified using antihuman CD45 antibody) in the bone marrow (BM), spleen, blood, or ascites collected from some of the mice treated or not (THP-1 columns,  $n = 4$ ) with DB1055 ( $n = 3$ ) or AraC ( $n = 3$ ). (D) Schedule of DB818 treatment of two million THP-1-Luc engrafted by IP route in NSG mice. (E) Quantification of the time course for bioluminescent THP-1-Luc responses to DB818 treatment in ventral orientation. Quantification is expressed in photons/second over time. (F) Spleen weight graph and (G) total quantification of THP-1 cells (hCD45-positive cells) per spleen from control mice (CTR, no THP-1), THP- inoculated mice further treated with vehicle (THP-1) or DB818. (H) Flow cytometry analysis of the percentage of human CD11b-positive cells within THP-1 cells (as identified with anti-human CD45 antibody) in bone marrow, liver, or blood samples of mice treated with vehicle (THP-1,  $n = 7$ ) or with DB818 ( $n = 5$ ). All results are presented as mean  $\pm$  SEM. Statistics, Student *t*-test: \*\*\* $p < 0.001$ ; \*\* $p < 0.01$ ; \* $p < 0.05$ ; ns, nonspecific or *p*-values as indicated in graphs.

evaluated for the treatment of THP-1 cells expressing the luciferase gene (Figure 8D). Treatment with DB818 did not affect mice weight (DB818 vs. “no cells”) whereas the presence of ascites increased mice body weight at the end of the protocol (Supporting Information S1: Figure 13a). In vivo bioluminescence imaging indicated a significant decrease in leukemia development over time (Figure 8E), associated with a decrease in spleen weight (Figure 8F and Supporting Information S1: Figure 13b,c) and the number of THP-1 (hCD45+) cells per spleen (Figure 8G). An increase in the percentage and/or median expression of hCD11b-positive THP-1 cells is also observed in the bone marrow, liver, blood, and ascites (Figure 8H and Supporting Information S1: Figure 13d–g). DB818 treatment also reduced splenomegaly associated with U937 xenograft in an in vivo model, and DB1055 was evaluated on the EOL-1 mice model, showing a potent reduction in splenomegaly, contrasting with the poor efficiency of AraC in this model (Supporting Information S1: Figure 14).

Therefore, the in vivo evaluations of HOXA9/DNA binding inhibitors demonstrate DB1055's efficacy in reducing THP-1-induced splenomegaly, while DB818 shows a significant decrease in leukemia development, underscoring their promising therapeutic potential in mouse models.

### DB818 and DB1055 treatments affect cell survival of blasts from AML patients in a HOXA9-dependent manner

A panel of 42 primary AML cells, obtained from the bone marrow or blood samples, underwent purification and assessment of HOXA9 expression by RT-qPCR and sensitivity to DB818 or DB1055 treatment (1–50  $\mu$ M). HOXA9 expression, presented atop the table, correlates with cytogenetic and/or molecular analyses for each patient (Figure 9A), revealing associations, such as MLL and NPM1 subtypes with HOXA9 overexpression, and cEBP $\alpha$ , Inv(16), and t(8-21) subtypes with low HOXA9 expression as expected from the literature<sup>1,6,10,14,16</sup> (Figure 9A). A positive correlation between AML blast cell survival upon DB818 treatment and HOXA9 expression was observed (Figure 9B). Moreover, the 50% more DB818-sensitive AML blast cells significantly expressed more HOXA9 mRNA than the 50% more resistant ones (Figure 9C). Sensitivity to DB818 also varied among different cytogenetic/molecular subtypes of AML, with the NPM1 or MLL HOXA9-overexpressing subtypes showing greater sensitivity compared to the HOXA9-negative cEBP $\alpha$  subtype (Figure 9D). Because primary cells cannot be maintained in culture for longer than 96 h and achieving long-term differentiation upon treatment with DB1055 might require extended incubation times, we evaluated the antileukemic activity of DB1055 in patient-derived xenografts in NSG mice, comparing it with AraC. Two AML patient blast cells from Figure 9A were subjected to the scheduled treatment presented in top panels of Figure 9E,F, based on a series of three

injections on Days 1, 3, and 5 with DB1055 or Ara-C followed by two weeks OFF (Figure 9E, PDX-1; Figure 9F, PDX-2). Three and four series of treatments were performed depending on the evolution of disease in the PDX-1 and PDX-2 untreated mice, respectively. Both DB1055 and Ara-C markedly and significantly reduced the AML-associated splenomegaly with no significant alterations in body weights observed (Supporting Information S1: Figure 15a,b). Furthermore, there was a notable reduction in the total blast cell count in spleens, bone marrows, and blood, underscoring the potential therapeutic effectiveness of DB1055 in patient-derived AML models (Figure 9E,F, Supporting Information S1: Figures 15a–g).

Overall, the study revealed a collective correlation between HOXA9 expression and cytogenetic/molecular subtypes, with DB818 sensitivity positively associated with HOXA9 expression, and noteworthy therapeutic effectiveness of DB1055 in patient-derived xenografts, resulting in the reduction of AML-associated splenomegaly and blast cell count.

## DISCUSSION

HOXA9 is crucial in various AML subtypes, including NPM1-mutated, MLL-rearranged, NUP98-NSD1, NUP98-HOXA9, and RUNX/EVI1 fusion subtypes,<sup>10,11,14,26</sup> yet lacks direct targeting for AML treatment. We identified two DNA-binding compounds, DB818 and DB1055, which can disrupt HOXA9-DNA interaction and restore AML cell differentiation. Selected from a diverse series of heterocyclic diamidines, including Pit-1 and Brn-3 (DB293),<sup>23</sup> ERG (DB1255),<sup>24</sup> and SPI1/PU.1 (DB1976, DB2115, DB2313),<sup>25</sup> DB818 and DB1055 exhibited strong in vivo antileukemic potential. Notably, DB2313 only demonstrated efficacy in mice injected with human AML pretreated cells. Our study underscores the promise of DB818 and DB1055 as potential therapeutics by targeting HOXA9 in AML.

This study establishes that HOXA9 knockdown and DB818 or DB1055 treatment decrease cell growth and survival while promoting cell death and restoring AML cell differentiation. Genes associated with cell proliferation, cell death, and myeloid cell differentiation show consistent deregulation. Notably, both DB818 and DB1055 proficiently affect the expression of the gene that evidenced direct HOXA9/DNA binding in the MV4-11 AML cell model,<sup>34</sup> as illustrated by HOXA9 ChIP-seq peaks localization on DNase-seq analyses (Figure 5 and Supporting Information S1: Figure 10).

DB818 and DB1055 induce myeloid cell differentiation both ex vivo and in vivo, supporting further development of DB1055 and DB818 as novel AML differentiation therapies. In vitro, DB818 was further evaluated against blast cells from 42 AML patients, revealing a correlation between DB818 sensitivity (IC<sub>50</sub>) and HOXA9 expression in AML blast cells (Figure 9) as it was shown for human AML cell lines (Figure 1A,B). It is worth noting that despite DB818 and DB1055 acting as competitors for HOXA9/DNA binding activity, cells





**FIGURE 9** Evaluation of the effect of the selected inhibitors on cell survival of blasts from patients and patient-derived xenografts (PDX) mouse models. (A) A series of 42 blast cells were obtained from acute myeloid leukemia (AML) patients. All samples are individually numbered and cytogenetically and molecularly defined according to patients' information referred to in Supporting Information S1: Table 3. All of the AML blast samples were quantified by quantitative reverse-transcription polymerase chain reaction for HOXA9 expression relative to TBP expression. Values presented from 12.45 to  $-12.4$  correspond to the individual  $\Delta C_t$  values for HOXA9 expression relative to that of the housekeeping gene TBP used as a normalization control. Moreover, means  $\Delta C_t$  from 2.9 to  $-11.4$  are calculated in the right column for each defined cytogenetically/molecularly different AML subtype defined on the left (the number of samples for each alteration is indicated as a value). This validates that our samples with the defined alterations are in agreement with known HOXA9-positive (such as NPM1 or MLL) or -negative (C/EBP $\alpha$ , inv(16), t(8;21) subtypes of AML). (B) Graph for correlation analysis between HOXA9 expression relative to TBP and DB818 response analyzed by diphenyltetrazolium bromide (MTT). The coefficient of determination and  $p$ -values are embedded in the graph. (C) Graph comparing the mean  $\pm$  SEM of individual  $\Delta C_t$  values (dots) for 50% more DB818-sensitive or -resistant AML samples determined using MTT assays after 96 h incubation with increasing concentrations of DB818 as defined in the Materials and Methods section. (D) Graph presenting the IC<sub>50</sub> of DB818 treatment (MTT assays at 96 h treatment) of AML blasts from NPM1 and MLL (HOXA9-positive subtypes) relative to cEBP $\alpha$ -mutated AMLs (HOXA9-negative subtype). (E, F) DB1055 treatment of PDX from two AML patient blasts cells (E) PDX-1: AML-M1, NPM1-mutated, Flt-3-ITD, IDH2-mutated, WT1+; (F) PDX-2: AML-M4, NPM1-mutated, Flt-3-TKD, IDH1-mutated, as indicated in Supporting Information S1: Table S3). Top: treatment schedules after intratibial (IT) injection of  $5 \times 10^6$  blast cells amplified in a first recipient mice series. Medium: measurement of spleens (middle pictures) and comparison of spleen weight (bottom graphs). Bottom: quantification of human CD45-positive (identifying human patient AML cells) per spleen or femur (bone marrow cells). Statistics, Student  $t$ -test: \*\*\* $p < 0.001$ ; \*\* $p < 0.01$ ; \* $p < 0.05$ ; ns, nonspecific.

expressing the highest level of HOXA9 do not appear as the less sensitive ones, suggesting that (i) the drug amount is sufficient to give an effect even if the expression of HOXA9 is high and (ii) this effect may be associated with different HOXA9 oncogenic-dependency of the cells and/or different sets of deregulated genes or level of deregulated expression depending on the AML cell lines or patient samples.

In vivo assessment of DB1055 on two AML patient-derived xenografts demonstrated antileukemic effects, with reduced spleen size and a lower number of hCD45-positive cells in the bone marrow (Figure 9E,F and Supporting Information S1: Figure 15).

Transcription factors, historically deemed “undruggable targets,” are seldom addressed in anti-tumor therapies. While ligand-like drugs, like ATRA against PML-RAR $\alpha$ , target nuclear/steroid-receptor family factors, the prevailing strategy involves interactions between transcription factors or with other proteins (e.g., p53/mdm2, RUNX1/CBF, Smad4/SKI, YAP/TAZ, COUP-TF, Smad2/3/4, BCL6 homodimers, HOX/PBX).<sup>9,19,35,36</sup> However, this method applies to specific couples with identified collaborators. Fewer inhibitors compete with a transcription factor's binding to its site consensus, like mithramycin inhibiting SP1/DNA interaction.<sup>37</sup> An ideal transcription factor for DNA-binding targeted therapy should be expressed selectively in cancer cells (ensuring a favorable therapeutic index) and directly linked to the oncogenic process as found in HOXA9 for AML. Given that conventional chemotherapy is still the standard AML treatment, the need for new targeted therapies, especially against various AML subtypes like those involving HOXA9, remains imperative. Among the newly approved or evaluated treatments,<sup>2,3</sup> differentiation therapies have indeed proved effective in the clinic such as the mitochondrial protein IDH2 (isocitrate dehydrogenase-2) inhibitor enasidenib (AG221, Celgene),<sup>5,38</sup> the IDH1 inhibitor ivosidenib (AG-120, Agios),<sup>5,39</sup> lysine-specific demethylase 1 (LSD1) inhibitors<sup>40,41</sup> such as tranylcypromine and analogs<sup>32,42</sup> or ORY-1001,<sup>3,43–45</sup> or the DOT1L inhibitor pinometostat (EPZ-5676)<sup>7,17,46,47</sup> known to down-regulate HOXA9 expression.<sup>48</sup> More recently the Menin/MLL inhibitor revumenib (SNDX-5613) showed promising results against the HOXA9-dependant MLL subtypes of AML,<sup>6,49</sup> but it also led to resistance.<sup>50</sup> Overcoming this resistance and other expected ones will require new drugs,<sup>3,4</sup> with one approach being the direct targeting of HOXA9 function as a common downstream effector of differentiation blockade.<sup>10</sup> HOXA9 is an interesting oncogenic target since it is not or only slightly expressed in healthy adult tissues, except in hematopoietic stem cells. Interestingly, our inhibitors did not show any major deleterious effects on human CD34+ hematopoietic stem cells and the survival and differentiation of progenitors (Figure 3). We hypothesize that HOXA9 could deregulate different sets of genes

between the maintenance of normal or leukemic stem cells, perhaps also via associations with different co-factors, to induce a cascade of differentiation and more rapid death on models of human AML than with human hematopoietic stem cells. The absence of a detrimental effect on normal hematopoiesis is an extremely interesting point for therapeutic strategies aimed at inhibiting HOXA9 function in the future.

In conclusion, the current findings support the potential of DB818 and DB1055 as promising candidates for a novel AML differentiation therapy. Inhibiting HOXA9/DNA interaction by DB818/1055 provides a means to disrupt the expression of genes implicated in blocking cell differentiation, offering a unique opportunity for future drug development.

## ACKNOWLEDGMENTS

Marie-Hélène David-Cordonnier expresses thanks to Elise Mozin, Amandine Deborgher, Xavier Dezitter, Marine Bellart, Lina Lutchmee, Lucie Louis-Thérèse, and Meryem Alliou for technical assistance in cellular experiments. Marie-Hélène David-Cordonnier is especially grateful to Mr. Denis Greuet for kindly passing on his technical expertise in the intra-tibial injection of mice and Dr. Thomas Boyer for expertise in cell morphology associated with the differentiation of AML cells. We also thank Sheherazade Sebda and Frédéric Leprêtre (Agilent platform of the University of Lille), Nathalie Jouy and Antonino Bongiovanni (Bicel platform of the University of Lille), and the EOPS1 animal facility members for assistance and expertise. David W. Boykin thanked Abdelbasset A. Farahat, Mohamed A. Ismail, and Arvind Kumar for DB818 and DB1055 compounds re-syntheses. The authors thank Prof. Christophe Roumier (Tumour bank: Tumourothèque du C2RC and Tumour Bank for the ALFA group, CHRU Lille, Biobanking declaration at the French Ministry of Research DC-2008-620, authorization granted by the French Ministry of Research AC-2013-1847, NF-S-96-900, Certificate Number: 2014/65453.1) for handling, conditioning, and storing patient samples. We are grateful to Dr. Nabeel Yaseen (Northwestern University, Chicago, USA) and Prof. Bob Weinberg for the kind gift of HOXA9 expressing vector and shLuc pRRL, respectively.

## AUTHOR CONTRIBUTIONS

Mélanie Lambert designed and performed cellular and in vivo experiments as well as transcriptomic analyses and wrote the manuscript. Samy Jambon participated in animal model experiments and evaluated hematological toxicity. Mohamed A. Bouhleb subcloned TY-HOXA9 and performed western blot analyses and DNase-seq

experiments. Sabine Depauw performed cellular and in vivo experiments. Julie Vrejin repeated some cellular experiments that comforted the experiments on THP-1 cell line differentiation. Samuel Blanck and Guillemette Marot analyzed DNase-seq data. Martin Figeac generated microarray and DNase-seq data from the genomic platform of the University of Lille. Claude Preudhomme and Bruno Quesnel provided AML patient samples and patient cytogenetic and molecular information (Lille Tumour Bank). David W. Boykin provided DB818 and DB1055. Marie-Hélène David-Cordonnier designed, supervised, participated in experiments, and wrote the manuscript.

### CONFLICT OF INTEREST STATEMENT

The authors declare no conflict of interest.

### DATA AVAILABILITY STATEMENT

The data that support the findings of this study are available from the corresponding author upon reasonable request.

### FUNDING

Marie-Hélène David-Cordonnier is grateful to the Ligue contre le Cancer-Septentrion (Comité du Nord, Comité du Pas-de-Calais), the Association Laurette Fugain (ALF-2016/05), the Association pour la Recherche sur le Cancer (ARC-SFI20111203669), the FEDER-Région Nord-Pas-de-Calais, the SIRIC ONCOLille (Axis-1 Tumor Dormancy), and the "Institut pour la Recherche sur le Cancer de Lille" (IRCL) for grants. David W. Boykin is grateful to the National Institutes of Health for Grant GM111749. Mélanie Lambert acknowledges the University of Lille, the French Research Ministry, and the Société Française d'Hématologie (SFH) for PhD fellowship. Samy Jambon expresses thanks to the ARC for PhD fellowship, while Mohamed A. Bouhrel to the IRCL and the Foundation de France for postdoctoral fellowships.

### ORCID

Samuel Blanck  <http://orcid.org/0000-0002-7868-2844>

Marie-Hélène David-Cordonnier  <http://orcid.org/0000-0001-9831-5577>

### SUPPORTING INFORMATION

Additional supporting information can be found in the online version of this article.

### REFERENCES

- Short NJ, Rytting ME, Cortes JE. Acute myeloid leukaemia. *Lancet*. 2018;392:593-606. doi:10.1016/S0140-6736(18)31041-9
- Choi JH, Shukla M, Abdul-Hay M. Acute myeloid leukemia treatment in the elderly: a comprehensive review of the present and future. *Acta Haematol*. 2023;146:431-457. doi:10.1159/000531628
- Turkalj S, Radtke FA, Vyas P. An overview of targeted therapies in acute myeloid leukemia. *Hemasphere*. 2023;7:e914. doi:10.1097/HS9.0000000000000914
- Santinelli E, Pascale MR, Xie Z, et al. Targeting apoptosis dysregulation in myeloid malignancies—the promise of a therapeutic revolution. *Blood Rev*. 2023;62:101130. doi:10.1016/j.blre.2023.101130
- Aiman W, Ali MA, Basit MA, et al. Efficacy and tolerability of isocitrate dehydrogenase inhibitors in patients with acute myeloid leukemia: a systematic review of clinical trials. *Leuk Res*. 2023;129:107077. doi:10.1016/j.leukres.2023.107077
- Issa GC, Aldoss I, DiPersio J, et al. The menin inhibitor revumenib in KMT2A-rearranged or NPM1-mutant leukaemia. *Nature*. 2023;615:920-924. doi:10.1038/s41586-023-05812-3
- Daigle SR, Olhava EJ, Therkelsen CA, et al. Potent inhibition of DOT1L as treatment of MLL-fusion leukemia. *Blood*. 2013;122:1017-1025. doi:10.1182/blood-2013-04-497644
- Bouhrel M, Lambert M, David-Cordonnier M-H. Targeting transcription factor binding to DNA by competing with DNA binders as an approach for controlling gene expression. *Curr Top Med Chem*. 2015;15:1323-1358. doi:10.2174/1568026615666150413154713
- Lambert M, Jambon S, Depauw S, David-Cordonnier MH. Targeting transcription factors for cancer treatment. *Molecules*. 2018;23:1479-1529. doi:10.3390/molecules23061479
- Lambert M, Alioui M, Jambon S, Depauw S, Van Seuningen S, David-Cordonnier MH. Direct and indirect targeting of HOXA9 transcription factor in acute myeloid leukemia. *Cancers*. 2019;11:837-874. doi:10.3390/cancers11060837
- Shenoy US, Adiga D, Alhedian F, Kabekkodu SP, Radhakrishnan R. HOXA9 transcription factor is a double-edged sword: from development to cancer progression. *Cancer Metastasis Rev*. Published online December 8, 2023. doi:10.1007/s10555-023-10159-2
- Golub TR, Slonim DK, Tamayo P, et al. Molecular classification of cancer: class discovery and class prediction by gene expression monitoring. *Science*. 1999;286:531-537. doi:10.1126/science.286.5439.531
- Grubach L, Juhl-Christensen C, Rethmeier A, et al. Gene expression profiling of Polycomb, Hox and Meis genes in patients with acute myeloid leukaemia. *Eur J Haematol*. 2008;81:112-122. doi:10.1111/j.1600-0609.2008.01083.x
- Gao L, Sun J, Liu F, Zhang H, Ma Y. Higher expression levels of the HOXA9 gene, closely associated with MLL-PTD and EZH2 mutations, predict inferior outcome in acute myeloid leukaemia. *Onco Targets Ther*. 2016;9:711-722.
- Nakamura T, Largaespada DA, Shaughnessy JD, Jenkins NA, Copeland NG. Cooperative activation of Hoxa and Pbx1-related genes in murine myeloid leukaemias. *Nat Genet*. 1996;12:149-153. doi:10.1038/ng0296-149
- Dorsam ST, Ferrell CM, Dorsam GP, et al. The transcriptome of the leukemogenic homeoprotein HOXA9 in human hematopoietic cells. *Blood*. 2004;103:1676-1684. doi:10.1182/blood-2003-07-2202
- Daigle SR, Olhava EJ, Therkelsen CA, et al. Selective killing of mixed lineage leukemia cells by a potent small-molecule DOT1L inhibitor. *Cancer Cell*. 2011;20:53-65. doi:10.1016/j.ccr.2011.06.009
- Kon Kim T, Gore SD, Zeidan AM. Epigenetic therapy in acute myeloid leukemia: current and future directions. *Semin Hematol*. 2015;52:172-183. doi:10.1053/j.seminhematol.2015.04.003
- Morgan R, El-Tanani M, Hunter KD, Harrington KJ, Pandha HS. Targeting HOX/PBX dimers in cancer. *Oncotarget*. 2017;8:32322-32331. doi:10.18632/oncotarget.15971
- Alharbi RA, Pandha HS, Simpson GR, et al. Inhibition of HOX/PBX dimer formation leads to necroptosis in acute myeloid leukemia cells. *Oncotarget*. 2017;8:89566-89579. doi:10.18632/oncotarget.20023
- Depauw S, Lambert M, Jambon S, et al. Heterocyclic diamidine DNA ligands as HOXA9 transcription factor inhibitors: design, molecular evaluation, and cellular consequences in a HOXA9-dependant leukemia cell model. *J Med Chem*. 2019;62:1306-1329. doi:10.1021/acs.jmedchem.8b01448
- Mdachi RE, Thuita JK, Kagira JM, et al. Efficacy of the novel diamidine compound 2,5-Bis(4-amidinophenyl)-furan-bis-O-Methylamidoxime (Pafuramidine, DB289) against *Trypanosoma brucei* rhodesiense infection in vervet monkeys after oral administration. *Antimicrob Agents Chemother*. 2009;53:953-957. doi:10.1128/AAC.00831-08
- Peixoto P, Liu Y, Depauw S, et al. Direct inhibition of the DNA-binding activity of POU transcription factors Pit-1 and Brn-3 by selective binding of a phenyl-furan-benzimidazole dication. *Nucleic Acids Res*. 2008;36:3341-3353. doi:10.1093/nar/gkn208
- Nhili R, Peixoto P, Depauw S, et al. Targeting the DNA-binding activity of the human ERG transcription factor using new heterocyclic dithiophene diamidines. *Nucleic Acids Res*. 2013;41:125-138. doi:10.1093/nar/gks971

25. Antony-Debré I, Paul A, Leite J, et al. Pharmacological inhibition of the transcription factor PU.1 in leukemia. *J Clin Invest.* 2017;127:4297-4313. doi:10.1172/JCI92504
26. Faber J, Krivtsov AV, Stubbs MC, et al. HOXA9 is required for survival in human MLL-rearranged acute leukemias. *Blood.* 2009;113:2375-2385. doi:10.1182/blood-2007-09-113597
27. LaRonde-LeBlanc NA, Wolberger C. Structure of HoxA9 and Pbx1 bound to DNA: Hox hexapeptide and DNA recognition anterior to posterior. *Genes Dev.* 2003;17:2060-2072. doi:10.1101/gad.1103303
28. Sonoda Y, Itoh M, Tohda S. Effects of HOXA9 Inhibitor DB818 on the growth of acute myeloid leukaemia cells. *Anticancer Res.* 2021;41:1841-1847. doi:10.21873/anticancer.14950
29. Godar S, Ince TA, Bell GW, et al. Growth-inhibitory and tumor-suppressive functions of p53 depend on its repression of CD44 expression. *Cell.* 2008;134:62-73. doi:10.1016/j.cell.2008.06.006
30. Daigneault M, Preston JA, Marriott HM, Whyte MKB, Dockrell DH. The identification of markers of macrophage differentiation in PMA-stimulated THP-1 cells and monocyte-derived macrophages. *PLoS One.* 2010;5:e8668. doi:10.1371/journal.pone.0008668
31. Ramos-Mejía V, Navarro-Montero O, Ayllón V, et al. HOXA9 promotes hematopoietic commitment of human embryonic stem cells. *Blood.* 2014;124:3065-3075. doi:10.1182/blood-2014-03-558825
32. Wass M, Göllner S, Besenbeck B, et al. A proof of concept phase I/II pilot trial of LSD1 inhibition by tranylcypromine combined with ATRA in refractory/relapsed AML patients not eligible for intensive therapy. *Leukemia.* 2021;35:701-711. doi:10.1038/s41375-020-0892-z
33. Wright S, Zhao X, Rosikiewicz W, et al. Systematic characterization of the HOXA9 downstream targets in MLL-r leukemia by noncoding CRISPR screens. *Nat Commun.* 2023;14:7464. doi:10.1038/s41467-023-43264-5
34. Zhong X, Prinz A, Steger J, et al. HoxA9 transforms murine myeloid cells by a feedback loop driving expression of key oncogenes and cell cycle control genes. *Blood Adv.* 2018;2:3137-3148. doi:10.1182/bloodadvances.2018025866
35. Gibault F, Bailly F, Corvaisier M, et al. Molecular features of the YAP inhibitor verteporfin: synthesis of hexasubstituted dipyrins as potential inhibitors of YAP/TAZ, the downstream effectors of the Hippo Pathway. *ChemMedChem.* 2017;12:954-961. doi:10.1002/cmdc.201700063
36. Bushweller JH. Targeting transcription factors in cancer—from undruggable to reality. *Nat Rev Cancer.* 2019;19:611-624. doi:10.1038/s41568-019-0196-7
37. Sleiman SF, Langley BC, Basso M, et al. Mithramycin is a gene-selective Sp1 inhibitor that identifies a biological intersection between cancer and neurodegeneration. *J Neurosci.* 2011;31:6858-6870. doi:10.1523/JNEUROSCI.0710-11.2011
38. Stein EM, DiNardo C, Altman JK, et al. Safety and efficacy of AG-221, a potent inhibitor of mutant IDH2 that promotes differentiation of myeloid cells in patients with advanced hematologic malignancies: results of a phase 1/2 trial. *Blood.* 2015;126:323. doi:10.1182/blood.V126.23.323.323
39. DiNardo C, de Botton S, Pollyea DA, et al. Molecular profiling and relationship with clinical response in patients with IDH1 mutation-positive hematologic malignancies receiving AG-120, a first-in-class potent inhibitor of mutant IDH1, in addition to data from the completed dose escalation portion. *Blood.* 2015;126:1306. doi:10.1182/blood.V126.23.1306.1306
40. Feng Z, Yao Y, Zhou C, et al. Pharmacological inhibition of LSD1 for the treatment of MLL-rearranged leukemia. *J Hematol Oncol.* 2016;9:24. doi:10.1186/s13045-016-0252-7
41. Harris WJ, Huang X, Lynch JT, et al. The histone demethylase KDM1A sustains the oncogenic potential of MLL-AF9 leukemia stem cells. *Cancer Cell.* 2012;21:473-487. doi:10.1016/j.ccr.2012.03.014
42. Teresa Borrello M, Benelkebir H, Lee A, et al. Synthesis of carbamide-containing tranylcypromine analogues as LSD1 (KDM1A) inhibitors targeting acute myeloid leukemia. *ChemMedChem.* 2021;16:1316-1324. doi:10.1002/cmdc.202000754
43. Maes T, Mascaró C, Tirapu I, et al. ORY-1001, a potent and selective covalent KDM1A inhibitor, for the treatment of acute leukemia. *Cancer Cell.* 2018;33:495-511. doi:10.1016/j.ccell.2018.02.002
44. Bose P, Konopleva MY. ORY-1001: overcoming the differentiation block in AML. *Cancer Cell.* 2018;33:342-343. doi:10.1016/j.ccell.2018.02.014
45. Salamero O, Montesinos P, Willekens C, et al. First-in-human phase I study of ladademstat (ORY-1001): a first-in-class lysine-specific histone demethylase 1A inhibitor, in relapsed or refractory acute myeloid leukemia. *J Clin Oncol.* 2020;38:4260-4273. doi:10.1200/JCO.19.03250
46. Klaus CR, Iwanowicz D, Johnston D, et al. DOT1L inhibitor EPZ-5676 displays synergistic antiproliferative activity in combination with standard of care drugs and hypomethylating agents in MLL-rearranged leukemia cells. *J Pharmacol Exp Ther.* 2014;350:646-656. doi:10.1124/jpet.114.214577
47. Rau RE, Rodriguez BA, Luo M, et al. DOT1L as a therapeutic target for the treatment of DNMT3A-mutant acute myeloid leukemia. *Blood.* 2016;128:971-981. doi:10.1182/blood-2015-11-684225
48. Zhang W, Zhao C, Zhao J, et al. Inactivation of PBX3 and HOXA9 by down-regulating H3K79 methylation represses NPM1-mutated leukemic cell survival. *Theranostics.* 2018;8:4359-4371. doi:10.7150/thno.26900
49. Wenge DV, Armstrong SA. The future of HOXA-expressing leukemias: menin inhibitor response and resistance. *Curr Opin Hematol.* 2023;31:64-70. doi:10.1097/MOH.0000000000000796
50. Perner F, Stein EM, Wenge DV, et al. MEN1 mutations mediate clinical resistance to menin inhibition. *Nature.* 2023;615:913-919. doi:10.1038/s41586-023-05755-9